CHARACTERIZATION OF MAGNETITE NANOPARTICLE REACTIVITY IN THE PRESENCE OF CARBON TETRACHLORIDE

April Marie Heathcock

Thesis submitted to the faculty of the Virginia Polytechnic Institute and State University in partial fulfillment of the requirements for the degree of

MASTER OF SCIENCE
In
Environmental Engineering

APPROVED:

Dr. Peter Vikesland
Dr. John Little
Dr. Marc Edwards

July 24, 2006
Blacksburg, Virginia

Keywords: Magnetite, Nanotechnology, Nanoparticle, Carbon Tetrachloride. Groundwater Remediation, Chlorinated Solvents

Characterization of Magnetite Nanoparticle Reactivity in the Presence of Carbon Tetrachloride

April Marie Heathcock

ABSTRACT

Throughout the United States, there are a large number of groundwater systems contaminated by chlorinated organic compounds. Of these compounds, carbon tetrachloride (CT) is one of the most frequently encountered due to its past, widespread industrial use. In anaerobic groundwater environments, CT has been shown to be susceptible to degradation by both biotic and abiotic processes. One abiotic process that has been researched extensively is the reduction of CT by iron metal and associated iron oxides and hydroxides. Magnetite, an iron oxide, is a ubiquitous component of many subsurface environments and has been investigated as a potential groundwater remediation technology. One beneficial characteristic of magnetite is the capability to be synthetically produced in various sizes and shapes - including particles within the nanoscale range. Nanoscale particles have been shown to be more reactive towards contaminants than larger sized particles due to their large surface areas and high surface reactivity. This project was designed to characterize the behavior of synthetic magnetite in the presence of carbon tetrachloride under anaerobic conditions.

ACKNOWLEDGEMENTS

I would like to especially thank my advisor, Dr. Peter Vikesland, for allowing me to work on this project and consequently broaden my knowledge and professional horizons. Thanks so much for your patience and assistance throughout this process.

Thank you to my committee members, Dr. Edwards and Dr. Little, for their input and advice and also to Jody Smiley and Julie Petruska for their laboratory expertise.

Very special thanks to Robert Rebodos and Erik Makus for all their assistance in the lab and input on this project.

Lastly, a special thanks to my parents, Alan and Elizabeth, for their unwavering support and to my fiancé, Chris, for his steadfast confidence.

GRANT INFORMATION

The National Science Foundation funded this project: Grant BES-053711.

TABLE OF CONTENTS

List of Table vi
List of Figures vii
List of Equations viii
Introduction 1
Materials And Methods 2
Particle Synthesis 2
Characterization of Synthesized Magnetite Nanoparticles 6
Chlorinated Organic Compounds 9
Dechlorination Reactions 9
Temperature Experiments 10
Results And Discussion 11
Kinetics of Carbon Tetrachloride Reduction 14
Particle Aggregation 20
    pH Effects 20
    Ionic Strength Effects 23
    Temperature 27
Conclusions 30
Literature Cited 31
Appendix A 34
  Yield Calculations
    Batch Yield 34
Maximum Yield 34
Appendix B 35
  Degradation and Formation Relationships
    Synthesis Reproducibility 35
    Temperature Dependence: 36
    Ionic Strength Dependence 37
    Mass Loading Dependence 39
    pH Dependency 41
Vita 42

LIST OF TABLES

Table 1. Summary of variables analyzed in kinetic experiments and particle conditions...5

Table 2. Chloroform yield percentages with corresponding electrolyte component and concentration.....27

LIST OF FIGURES

Figure 1. Reproducibility of Suspension Preparation 7
Figure 2. Zeta Potential Relationship for Nanomagnetite 8
Figure 3. Proposed Pathway for Reductive Dehalogentation of Carbon Tetrachloride 13
Figure 4. Change in Carbon Tetrachloride, Chloroform, and Carbon Monoxide Concentrations Over Time in the Presence of Nanomagnetite. 15
Figure 5. Carbon Tetrachloride Dechlorination Rates as a Function of Magnetite Particle Loading 18
Figure 6. Size Determination Using TEM Photography
A) TEM Images 19
B) Histogram of Non-Reacted Synthetic Magnetite 19
Figure 7. Normalized, Carbon Tetrachloride Reduction Rate Constants
A) Mass Normalized 22
B) Surface Area Normalized 22
Figure 8. Effect of Ionic Composition on the Pseudo-First Order Rate Constants
A) Carbon Tetrachloride Dechlorination 26
B) Chloroform Production 26
Figure 9. Arrhenius Plot of Carbon Tetrachloride and Chloroform Temperature Rate Dependence. 29
Figure 10. Synthesis Reproducibility 34
Figure 11. Temperature Dependence 35
Figure 12. Ionic Strength Dependence: Sodium Chloride 36
Figure 13. Ionic Strength Dependence: Calcium Chloride 37
Figure 14. Ionic Strength Dependence: Sodium Perchlorate 38
Figure 15. Mass Loading Dependence: pH 6 39
Figure 16. Mass Loading Dependence: pH = 7.8 40
Figure 17. pH Dependence. 41

LIST OF EQUATIONS

Equation 1. Reaction Of Magnetite And Carbon Tetrachloride 11
Equation 2. Rate Relationship For Magnetite And Carbon Tetrachloride.....14
Equation 3. Kinetic Rate For Carbon Tetrachloride 14
Equation 4. Observed Reaction Rate Coefficient 16
Equation 5. Mass Normalized Observed Reaction Rate.....16
Equation 6. Surface Area Normalized Observed Reaction Rate 16
Equation 7. Relation Of Mass To Surface Area Normalization 16
Equation 8. Chloroform Yield 24
Equation 9. Arrhenius Equation.....27

INTRODUCTION

Throughout the United States, there are a large number of groundwater systems contaminated by chlorinated organic compounds. Of these compounds, carbon tetrachloride (CT) is one of the most frequently encountered due to its past, widespread industrial use[1]. In anaerobic groundwater environments, CT has been shown to be susceptible to degradation by both biotic [2-4] and abiotic [5-14] processes. One abiotic process that has been studied extensively is the reduction of CT by iron metal and associated iron oxides and hydroxides [5-9, 11, 13, 15-17]. Magnetite, an iron oxide, is a ubiquitous component of many subsurface environments [18] and is formed through both natural and anthropogenic processes. As well as being a constituent of iron rich soils, magnetite is also formed through the corrosion of iron permeable reactive barriers [16] and by the action of dissimilatory iron-reducing bacteria [4]. Magnetite is a known reductant of carbon tetrachloride and has been studied as a potential remedial technology for contaminated groundwater systems [4, 19]. One beneficial characteristic of magnetite is the capability to be synthetically produced in various sizes and shapes - including particles within the nanoscale range (1-100 nm). Nanoscale particles have been shown to be more reactive towards contaminants than larger sized particles due to their large surface areas and high surface reactivity [20, 21]. Nanoparticles are also thought to have a great flexibility for in situ applications due to their ability to be delivered as particle slurry. Previous research has shown that pH can strongly influence the dechlorination rates of CT and also the subsequent product formation [19]. So it is desirable to understand what factors and mechanisms influence this system. This project was designed to characterize synthetic nanomagnetite in the presence of carbon tetrachloride

and to identify and analyze the primary variables that influence reactivity.

MATERIALS AND METHODS

All solutions were prepared using de-aerated, deionized water (> 18.1 MΩ) obtained from a Barnstead Nanopure filtration system. Water was de-aerated by boiling for 30 minutes and then sparging with either argon or nitrogen gas for an additional 30 minutes while boiling continued. De-aerated water was removed from the heating source, capped, and when cool enough to safely transport, was transferred to an anaerobic chamber. Reagent grade chemicals were used in all experiments and were obtained from Fisher Scientific.

Particle Synthesis

Magnetite was synthesized in the 95%/5% N_2/H_2 atmosphere of an anaerobic glovebox (Coy Laboratory Products Inc.) Using a method adapted from Vayssieres et al., magnetite was precipitated by drop-wise (~1 drop/s) addition of a mixture of 0.2 M ferric chloride and 0.1 M ferrous chloride to a well-mixed solution of 1 M sodium hydroxide in 1 M sodium chloride [22]. The overall ratio of iron solution to base solution was kept at 3:2 to keep the final pH of the mixture above 12. Continuous mixing was achieved and maintained throughout the synthesis by use of an overhead mixer, glass stirring shaft, and PTFE stirring blade. To remove excess salts, the precipitated nanoparticles were magnetically separated, decanted, and rinsed with de-aerated nanopure water a minimum of three times. Following the final rinse, the particles were brought to volume with water and stored in a polypropylene container in the anaerobic glovebox until use. The final pH of the stored particle solution was between 10.5 and 11.5. The salts used for each solution

were measured outside the glovebox, transferred to the chamber, and brought to volume with de-aerated water. Each salt solution was prepared fresh for each synthesis.

The yield of magnetite for each suspension was determined by drying a known volume of magnetite solution for >24 hours in a 75 °C oven. The dry particle mass was measured and divided by the aliquot volume to determine the concentration of particles in g/L. This particle mass was then converted into moles of Fe_3O_4 by considering the addition of oxygen to the particles as they dry and are converted into maghemite (γ-Fe_2O_3; see example calculation in Appendix A) [18]. Yield calculations were done assuming 100% conversion of Fe_3O_4 to γ-Fe_2O_3. Mass measurements were done in triplicate to calculate an average magnetite concentration for a given batch.

Penn et al. observed that in solution, the aggregation of iron oxide nanoparticles increases over time [23]. To minimize possible aging affects on particle reactivity, nanoparticles were generally prepared specifically for a given experiment. Table 1 provides information on the different batches of nanoparticles used and the conditions for each of the kinetic experiments.

Table 1. Summary of variables analyzed in kinetic experiments and particle conditions

Experiment Variable	Particle Batch		Ionic Strength (M)	Particle Mass Loading (g/L)	Temp (°C)	pH	Carbon Tetrachloride			Chloroform Formation	Carbon Monoxide Formation
							k_{obs} (hr^{-1})[1]	k_M (L g^{-1} hr^{-1})	k_{SA} (L m^{-2} hr^{-1})	k_{obs} (hr^{-1})	k_{obs} (hr^{-1})
Batch Consistency	I,II,III		0.1	5	22 ± 1°	7	0.041 ± 0.003 0.048 ± 0.002 0.048 ± 0.003	0.008 0.010 0.010	0.00013 0.00015 0.00015	0.165 ± 0.076 0.174 ± 0.095 0.046 ± 0.118	0.042 + 0.076 0.046 + 0.095 0.048 + 0.118
Nanoparticle Mass Loading	X		0.001	1 3 5 7 10	22 ± 1°	7.8	0.016 ± 0.004 0.100 ± 0.009 0.186 ± 0.009 0.298 ± 0.013 0.409 ± 0.019	0.005 0.003 0.004 0.004 0.005	0.00008 0.00004 0.00006 0.00006 0.00007	0 $4.7x10^{-6}$ ± 0.005 0.045 ± 0.009 0.059 ± 0.007 0.104 ± 0.021	not measured
	X		0.001	1 3 5 7 10	22 ± 1°	6	0.009 ± 0.001 0.010 ± 0.001 0.016 ± 0.001 0.019 ± 0.001 0.026 ± 0.002	0.009 0.003 0.003 0.003 0.003	0.00014 0.00005 0.00005 0.00004 0.00004	0.026 ± 0.012 0.145 + 0.016 0.240 ± 0.034 0.341 ± 0.054 0.368 ± 0.074	not measured
Ionic Strength (NaCl)	VIII		0.001 0.01 0.1 1	5	22 ± 1°	7.8	0.511 ± 0.025 0.267 ± 0.024 0.186 ± 0.006 0.125 ± 0.007	0.102 0.053 0.037 0.025	0.00161 0.00084 0.00059 0.00039	0.389 ± 0.064 0.203 ± 0.035 0.156 ± 0.029 0.140 ± 0.055	not measured
Ionic Strength ($CaCl_2$)	VIII		0.001 0.01 0.1 1	5	22 ± 1°	7.8	0.261 ± 0.025 0.259 ± 0.019 0.180 ± 0.007 0.151 ± 0.008	0.052 0.052 0.036 0.030	0.00082 0.00082 0.00057 0.00048	0.313 ± 0.174 0.281 ± 0.143 0.226 ± 0.082 0.135 ± 0.047	not measured
Ionic Strength ($NaClO_4$)	IX		0.001 0.01 0.1 1	5	22 ± 1°	7.8	0.696 ± 0.012 0.574 ± 0.012 0.285 ± 0.006 0.127 ± 0.008	0.139 0.115 0.057 0.025	0.00219 0.00181 0.00090 0.00040	0.424 ± 0.065 0.316 ± 0.032 0.205 ± 0.015 0.120 ± 0.008	not measured
Temperature	X	Roller Mixer	0.001	5	3.6 22	7.8	0.062 ± 0.006 0.197 ± 0.003	0.012 0.0393	0.00020 0.00062	0.101 ± 0.011 0.228 ± 0.012	not measured
		Water Bath			22 30 36		0.110 ± 0.007 0.339 ± 0.018 0.729 ± 0.017	0.022 0.068 0.146	0.00035 0.00107 0.00230	0.162 ± 0.011 0.421 ± 0.024 0.996 ± 0.096	
pH	VIII		0.001	5	22 ± 1°	6 6.5 7 7.5 8 8.5	0.012 ± 0.002 0.067 ± 0.007 0.189 ± 0.018 0.246 ± 0.023 0.518 ± 0.017 0.603 ± 0.013	0.002 0.013 0.038 0.049 0.104 0.121	0.00004 0.00021 0.00059 0.00077 0.00163 0.00190	0.168 ± 0.005 0.059 ± 0.003 0.151 ± 0.009 0.302 ± 0.048 0.663 ± 0.131 0.687 ± 0.216	not measured

[1] Standard errors are presented in conjunction with observed rate constants (k_{obs})

Characterization of Synthesized Magnetite Nanoparticles

To determine the reproducibility of the suspension preparation procedure, three separate batches were synthesized and their reactivity towards carbon tetrachloride was compared. As shown in Figure 1, the three batches exhibit similar reactivity towards carbon tetrachloride. This similarity indicates that differences in particle reactivity caused by batch-to-batch variability are minor.

The crystal structures of the particles were examined using an automated powder X-ray diffractometer (XRD) with CuKα radiation (analysis by XRD.US). Samples were prepared by allowing the particles to dry in an anaerobic glovebox for ~7 days. During this time period, the samples were periodically placed in a 70 °C oven to expedite the drying process.

The magnetite particle size was determined using Brunauer-Emmett Teller (BET) surface area analysis and transmission electron microscopy (TEM). The surface area of the synthesized particles was determined using N_2 physisorption and the multipoint BET method with a PMI Sorptometer (ABET series; analysis by Porous Media Inc.). Samples were prepared using the method described above for XRD analysis. The morphology of both reacted and non-reacted particles was determined using a Philips 420T TEM, at 100 kV. Collected images were transferred onto 3 ¼ × 4 ¼ negatives or digitally captured using a slow scan 3086 × 2056 pixel camera. Particles were mounted on carbon coated TEM grids and allowed to dry in an aerobic environment for a minimum of 48 hours to ensure all fluids were removed from the sample.

The point of zero charge (PZC) of the magnetite suspensions was evaluated using a Malvern Zetasizer 3000 HS. A series of aqueous magnetite suspensions with initial pH values ranging from pH 4.5-12, were analyzed to determine their respective zeta potentials. The PZC value was estimated by the graphical relationship between the measured zeta potential and the pH of the solution (Figure 2). Particle agglomeration is minimized at pH values near/at the PZC, while dispersion potential increases with increasing ΔpH from the PZC [24].

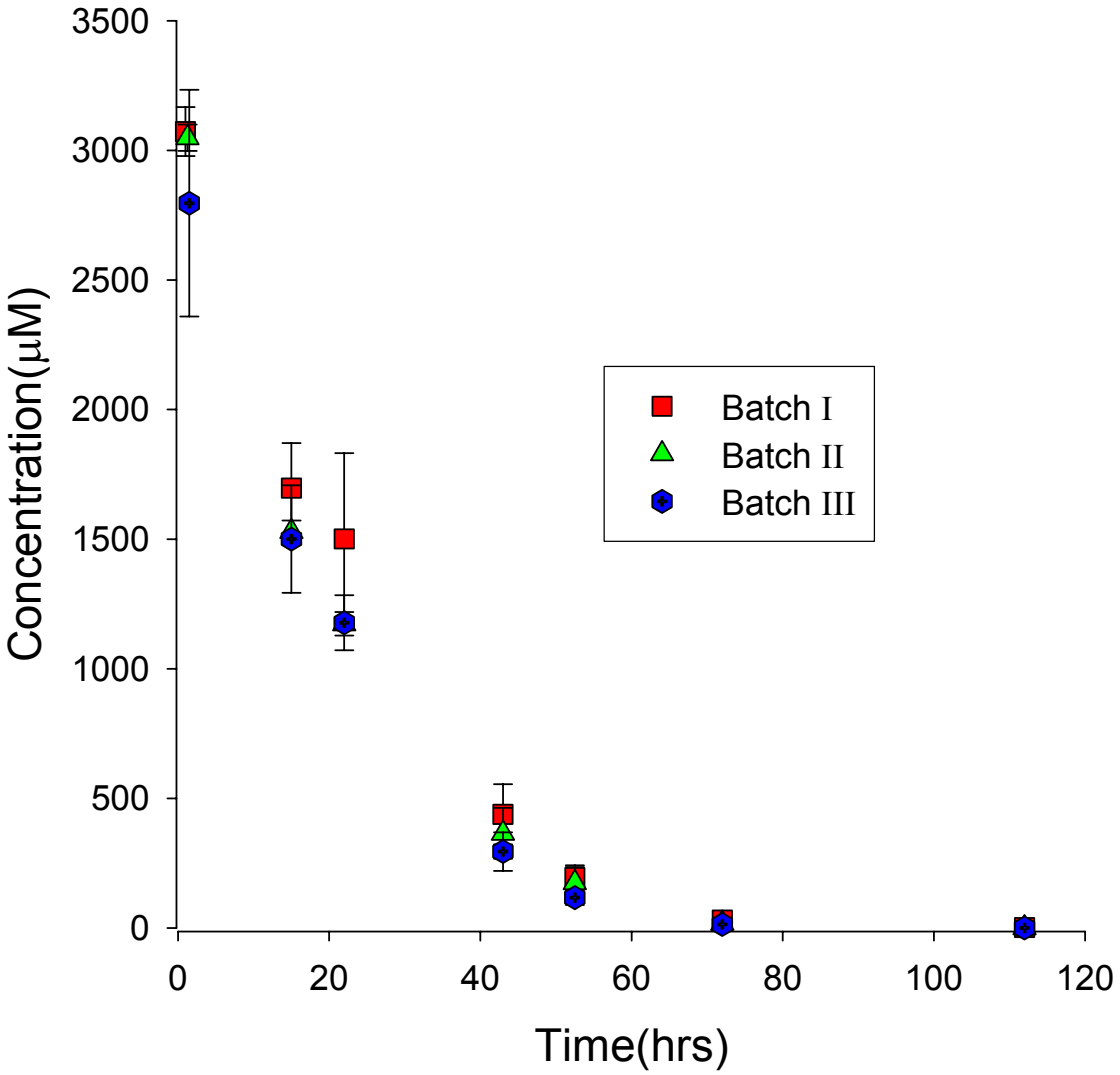

Figure 1. Reproducibility of Suspension Preparation; $[CT]_0$ = 3000 μM, pH = 7, 5 g/L Magnetite, 0.1 M NaCl, and 50 mM HEPES.

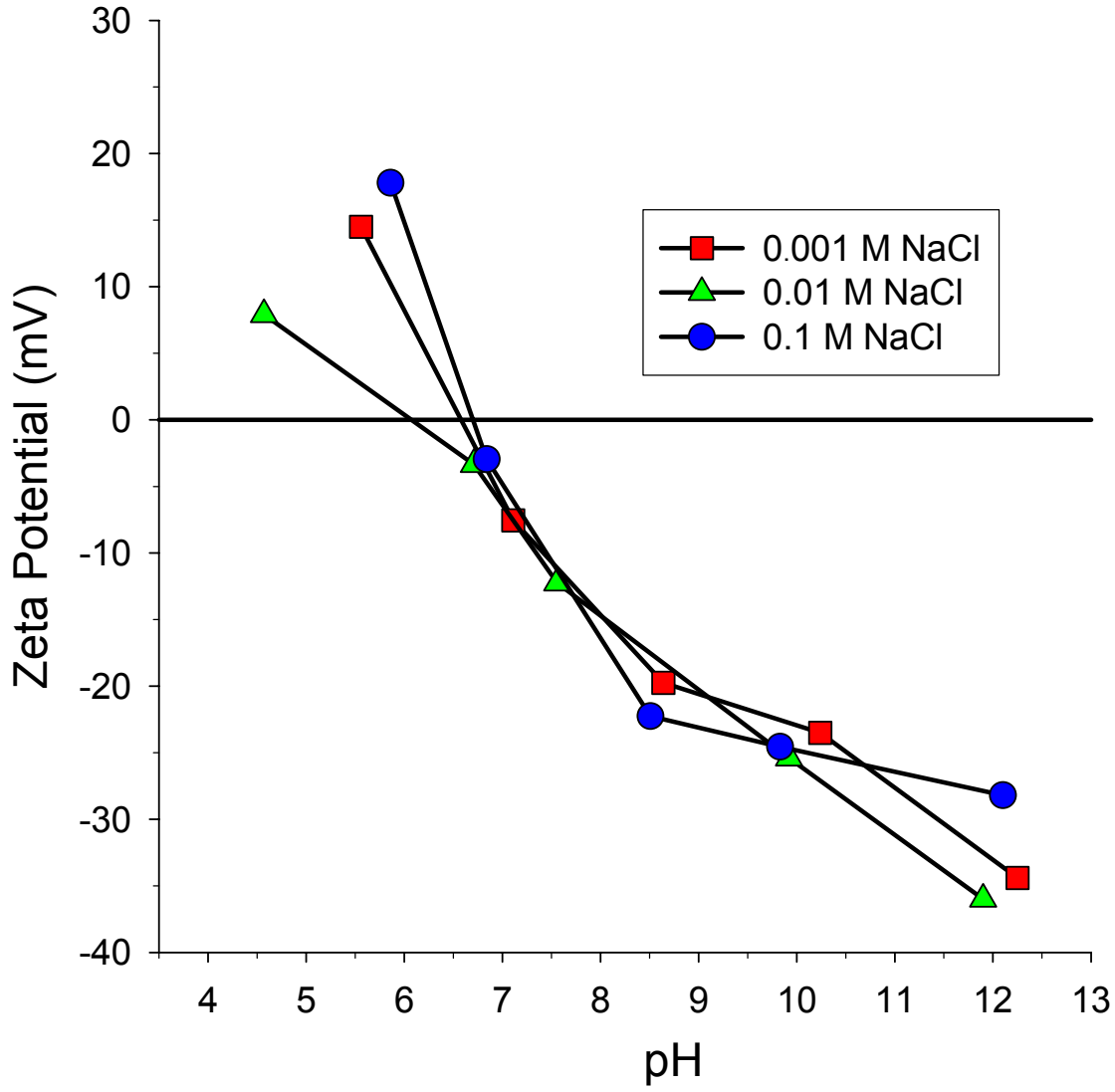

Figure 2. Zeta potential relationship for nanomagnetite, measured at three different ionic strengths. 120 mg/L Magnetite. (Data provided by Robert Rebodos)

Chlorinated Organic Compounds

Kinetic experiments were conducted by exposing magnetite nanoparticle solutions to chlorinated organic compounds. Carbon tetrachloride was chosen as the model contaminant due to its prevalence in the environment and the extensive amount of research that has gone into describing the reductive dehalogenation of CT in the presence of iron materials [3, 4, 7, 8, 11, 14, 19, 25]. Chloroform (CF) is one of the primary products formed by the reduction of CT, so kinetic experiments were also conducted with CF to determine if the particles could also reduce CF. One kinetic experiment was conducted using trichloroethylene (TCE) to determine if magnetite could reduce this compound. The experiments with both CF and TCE indicated that neither compound was readily reduced by nanomagnetite over the course of 120 hours. Accordingly, no further experiments were conducted with these compounds.

Dechlorination Reactions

All reactivity experiments were carried out in ~61 mL glass vials that were stored in the anaerobic chamber and allowed to equilibrate in the N_2/H_2 atmosphere for a minimum of 24 hours prior to use. The reactor vials were prepared by mixing an aliquot of magnetite stock solution with 50 mM HEPES (4-(2-hydroxyethyl)-1-piperazineethanesulfonic acid, purity >99% buffered water at a given ionic strength. Sodium chloride was the primary salt used to set the ionic strength; however, calcium chloride ($CaCl_2 \bullet 2H_2O$) and sodium perchlorate ($NaClO_4 \bullet H_2O$) were also employed. Particle concentrations ranged from 1-10 g/L, with the majority of the experiments conducted at a concentration of 5 g/L. The reactor pH was set by adding either 120 mM sodium hydroxide or 120 mM hydrochloric acid into each reactor until the desired pH was achieved. Upon pH stabilization, any remaining headspace was eliminated by the addition of de-aerated water. The vials were then capped and sealed with aluminum seals and septa. Prepared vials were equilibrated for a period of 8-96 hours prior to spiking them with an aliquot of CT, CF, or TCE (each in 100% methanol) to

achieve an initial concentration of ~ 100 μM. Following addition of each compound, the reactors were removed from the glovebox, placed on a bottle roller and mixed at a constant rpm until the desired sampling time. Prior to sampling, the reactors were taken off the roller mixer and placed on a magnet to enhance particle separation. At that point 250 μL of supernatant was withdrawn from the reactors, replaced with 250 μL of de-aerated water, and mixed with 2.75 mL of DI water in a 20 mL glass headspace autosampler vial. The vials were capped and sealed with aluminum caps and septa. Control reactors without magnetite were set up for each experiment under identical solution conditions.

Temperature Experiments

Dechlorination reactions were conducted over a range of temperatures to observe the affect of temperature on particle reactivity. The temperatures analyzed were 3.6, 22 (ambient), 30, and 36 °C. The temperatures were achieved with either a heated or ambient temperature water bath for the three higher temperatures, or refrigeration for the low temperature. The reactor vials were equilibrated at a designated temperature for ~8 hrs prior to CT addition. Mixing of the reactor vials was achieved by a bottle roller at 3.6 and 22 °C, and the rotating mechanism of the water bath at 22, 30, and 36 °C. The 22 °C reactions were carried out using both mixing devices in order to make apparent any inherent differences incorporated by using the different mixing regimes. Comparison of the observed rates measured for the 22 °C experiments, illustrates that there were significant differences in measured reaction rates for the two different mixing regimes. This result suggests that mixing effects play a role in the reaction kinetics. Based on this observation, detailed analysis of the temperature data was conducted using only experimental data acquired using the water bath mixed reactors. Additional studies of these mixing effects are planned for the future.

GC Operation Parameters

The CT, CF, and TCE concentrations were quantified by headspace analysis using a headspace gas analyzer (Finnigan Trace GC Ultra) with a 60 m × 0.32 mm capillary column (GS-Gaspro) and an electron capture detector (ECD). Temperature conditions were as follows: For CT and CF, initial oven temperature of 100 °C with a hold of 5 minutes, a ramp of 9 °C/min to 180 °C and hold of 2 minutes, a ramp of 20 °C/min to 200 °C and hold of 1 minute. For TCE, initial oven temperature of 125 °C with hold of 4 minutes, a ramp of 9 °C/min to 165 °C and hold for 2 minutes, a ramp of 10 °C/min to 225 °C and hold of 3 minutes. Carbon Monoxide (CO) was measured on a RGA 5 reduced gas analyzer (Trace Analytical) with a bed temperature of 265 °C and a column temperature of 80 °C. Nitrogen was used as the carrier and actuator gases at 275 kPa and 414 kPa, respectively.

RESULTS AND DISCUSSION

The reaction between magnetite (Fe_3O_4) and carbon tetrachloride can be expressed by the following:

$$Fe_3O_4 + CCl_4 \rightarrow \gamma - Fe_2O_3 + Fe^{2+} + \text{products} \qquad \textbf{(Equation 1)}$$

This reaction produces maghemite (γ-Fe_2O_3) a ferric iron oxide, ferrous iron, and a number of carbonaceous products. The products produced are a result of the reductive dehalogenation of carbon tetrachloride and can include a variety of intermediates whose relative proportions depend upon the electron transfer pathway that product formation follows [3, 19]. Figure 3, illustrates the proposed pathways for reductive dechlorination of carbon tetrachloride in the presence of magnetite.

Chloroform is the proposed end product of hydrogenolysis, which is a process widely accepted to be initiated by dissociative electron transfer. This means that the addition of the first electron to the CT molecule causes a dissociation of the molecular structure resulting in the

formation of the trichloromethyl free radical ($\bullet CCl_3$) and chloride [3, 26]. CF then forms from proton addition or •H abstraction [19]. Carbon monoxide and formate are endproducts formed by carbene hydrolysis and carbene reduction, respectively [3, 19]. It is unclear exactly what factors dictate the electron transfer pathway that product formation follows, but it is desirable to characterize product formation since chloroform is considered more toxic and recalcitrant in anaerobic environments than carbon tetrachloride [6].

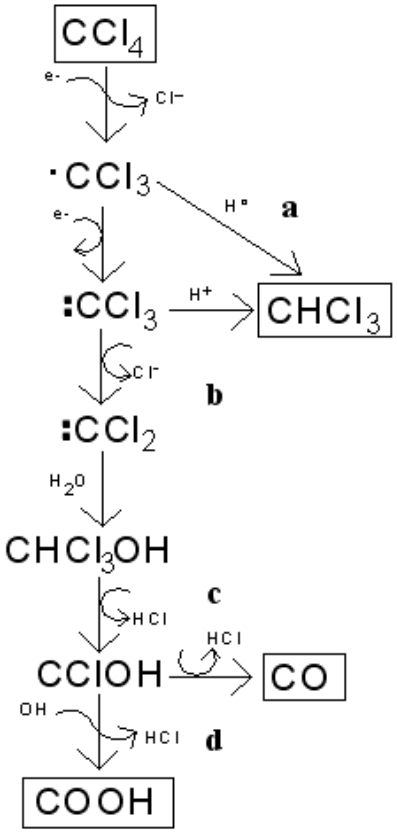

Figure 3. Proposed pathway for reductive dehalogentation of carbon tetrachloride in the presence of magnetite. Pathways a and b yield chloroform, the hydrogenolysis product; pathway c shows carbon monoxide formation via carbene hydrolysis; pathway d shows the pH dependent formate formation via carbene reduction; The boxes indicate the proposed stable end products.

Kinetics of Carbon Tetrachloride Reduction

Carbon tetrachloride readily reacts with nanomagnetite to produce chloroform and carbon monoxide. For the limited number of experiments where both CF and CO were monitored, CF production typically accounted for 60-80% of the initial carbon in CT, while CO production accounted for 15-20% of the initial carbon (Figure 4). For this project, CT and CF were the primary compounds monitored throughout the reactions. CO was only monitored in one experiment.

The kinetics of CT loss in the presence of magnetite can be modeled by a second-order model wherein the disappearance of CT is proportional to the dissolved CT concentration and the number of magnetite surface sites available for reaction:

$$\frac{d[\mathrm{CT}]}{dt} = -k_{\mathrm{CT}}[\mathrm{Fe_3O_4\ surface\ sites}]^{\alpha}[\mathrm{CT}]^{\beta} \qquad \textbf{(Equation 2)}$$

In this relationship k_{CT} is the overall second-order rate constant for CT loss, [CT] is the carbon tetrachloride concentration at time t, [Fe_3O_4 surface sites] is the magnetite surface site concentration, and α and β are the reaction orders with respect to [Fe_3SO_4 surface sites] and [CT], respectively. A pseudo-first-order rate expression can be developed from equation 2 by assuming the number of magnetite surface sites greatly exceeds the initial concentration of CT

$$\frac{d[\mathrm{CT}]}{dt} = -k_{\mathrm{obs}}[\mathrm{CT}] \qquad \textbf{(Equation 3)}$$

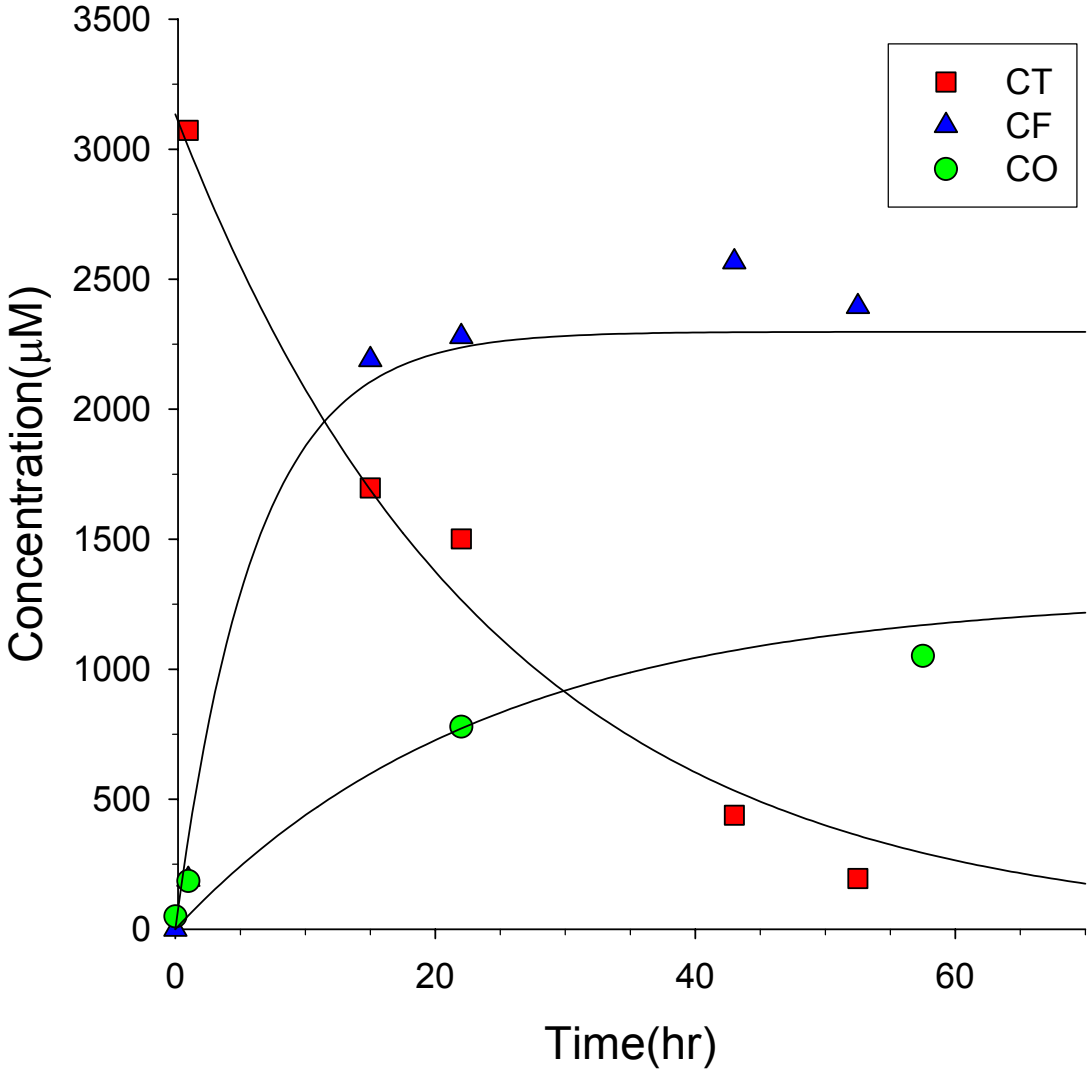

Figure 4. Change in carbon tetrachloride, chloroform, and carbon monoxide concentrations over time in the presence of nanomagnetite. The reactions were modeled with first-order regression analysis. $[CT]_0$ = 3 mM pH = 7, 5 g/L magnetite, 0.1 M NaCl, and 50 mM HEPES.

Combining equations (2) and (3) yields the expression for the observed pseudo-first order rate constant, k_{obs}:

$$k_{obs} = k_{CT}\left[Fe_3O_4 \text{ surface sites}\right]^{\alpha} \quad \textbf{(Equation 4)}$$

For this study, the formation of CF and CO was assumed to follow a pseudo-first order kinetic model. To check the validity of this assumption, the log concentration versus time relationship was plotted (data not shown) and based on the resultant linear relationship, the formation of CF and CO follows a first-order model. k_{obs} values and the associated standard errors for CT, CF, and CO were obtained by non-linear regression of concentration versus time data using the statistical package provided in SigmaPlot 8.0 and 9.0 and are tabulated in Table 1. Time courses and model fits may be found in Appendix B.

Assuming the system is first order with respect to the magnetite loading, k_{obs} can be expressed as a function of particle mass loading and the magnetite surface area:

$$k_{obs} = k_M\,[Fe_3O_4(g/L)] \quad \textbf{(Equation 5)}$$

$$k_{obs} = k_{SA}[\text{Surface Area of } Fe_3O_4\ (m^2/L)] \quad \textbf{(Equation 6)}$$

where k_M (L $g^{-1}hr^{-1}$) is the mass normalized rate coefficient, k_{SA} (L $m^{-2}hr^{-1}$) is the surface area normalized rate coefficient, and $[Fe_3O_4(g/L)]$ is the mass loading of magnetite for a particular system. Combining equations 5 and 6 and substituting variables for particle density (ρ_M) and surface area (a_S) yields the following relationship, which relates k_M to k_{SA}:

$$k_M \rho_M = k_{SA} a_S \rho_M \quad \textbf{(Equation 7)}$$

Mass loading experiments were conducted to assess the validity of this first order assumption and to determine the mass normalized rate coefficients. The reaction was confirmed to be first-order with respect to magnetite due to the linear increase in the CT dechlorination rate with an increasing particle load (Figure 5). The effects of particle loading on carbon tetrachloride reduction were assessed by varying the magnetite concentration between 1 and 10 g/L at both pH 6 and pH 7.8. For

both pH conditions, there was an increase in the observed CT dechlorination rate with increasing mass load. k_M values were determined from the slope of the relationship between k_{obs} and mass loading and were determined to be 0.002 L/g/hr and 0.044 L/g/hr for CT dechlorination at pH 6 and 7.8, respectively (Figure 5).

The surface area of the synthesized magnetite produced for this project was determined by two separate and independent methods: TEM and BET analysis. The mean geometric surface area was calculated by measuring the diameters of particles in a TEM image and assuming spherical particle geometry from a TEM image (Figure 6) and is reported to be 121.3 m^2/g. The surface area measured through BET gas adsorption is reported to be 63.5 m^2/g. Both analyses are accepted techniques for characterizing nanoparticle size. However it is apparent that these methods produce widely different results. These differences can be attributed to the methods used for sample preparation and analysis. TEM images should be a more accurate representative of a particle suspension since they are simply snapshots of the dried particles, but there are errors associated with making calculations from an image. BET analysis does not accurately reflect the characteristics of particle in suspensions, because the particles must be dried and then pulverized into a powder form for analysis. These differences suggest that a surface area normalization scheme should be adopted with great care since the potential exists for artifacts to taint the experimental results.

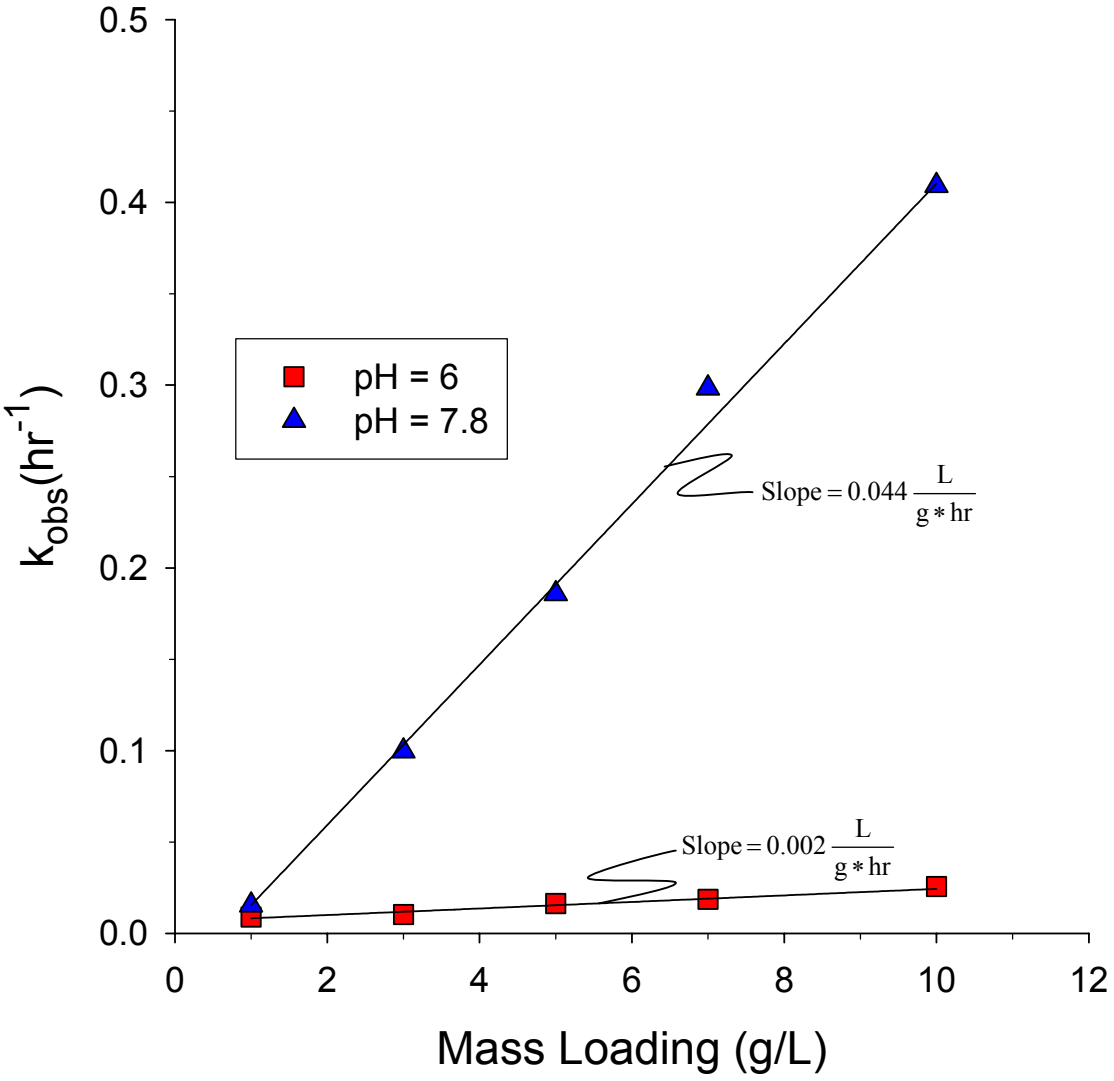

Figure 5. Carbon tetrachloride dechlorination rates as a function of magnetite particle loading. $[CT]_0$ = 100µM, 0.001 M NaCl and 50 mM HEPES.

A)

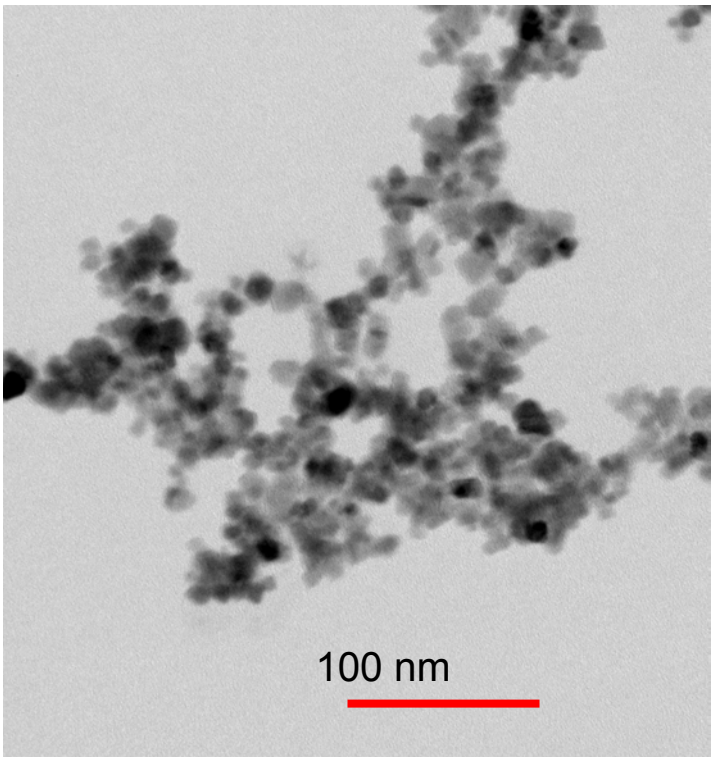

B)

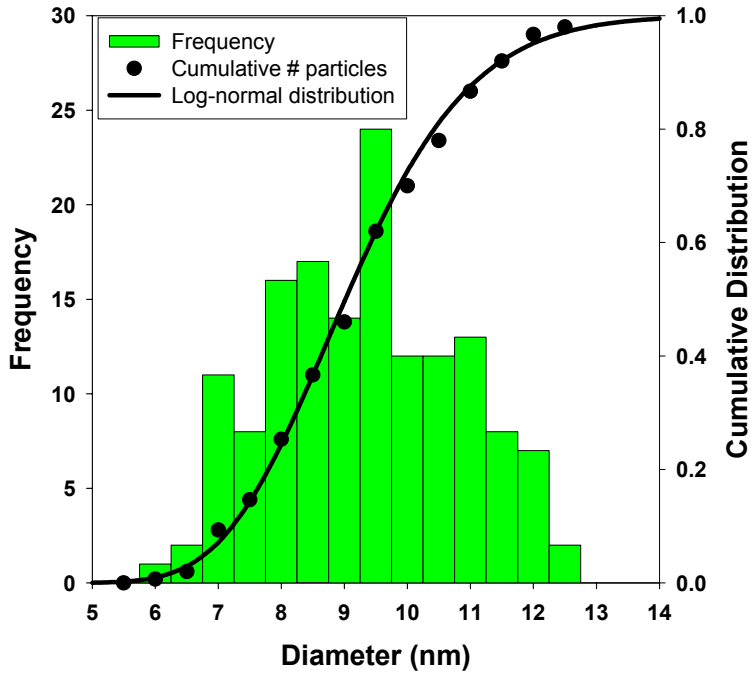

Figure 6. Size determination using TEM photograpy A) TEM images and B) Histogram of non-reacted synthetic magnetite: mean particle diameter determined by particle size analysis of TEM images = 9.2 ± 1.6 nm (n = 150)

Particle Aggregation

In aqueous suspensions, magnetite nanoparticles behave like magnetic colloids meaning that particle interactions are governed by both magneto-dipole forces and van der Waals forces [27]. Due to these interparticle reactions, multiparticle agglomerations form and often settle out of solution. This is problematic in terms of the characterization of these systems because an agglomerated system behaves differently than a dispersed system in terms of both particle mobility and surface characteristics [27]. Furthermore, it is unclear whether the system reflects the properties of the nano-constituents or displays unique properties of the bulk aggregate [28]. When attempting to characterize magnetite nanoparticle suspensions it is therefore desirable to determine and understand what factors influence these particle interactions and govern suspension stability. Previous research suggests that ionic strength and pH are two of the master variables that affect the aggregation/dispersion potential of a particle solution [20, 22, 23, 24]. pH has also been shown to directly affect CT reaction rates in the presence of magnetite [19]; however, the dependence of the reaction rate on ionic strength has not been previously explored for nanoparticle suspensions.

pH Effects

Magnetite, both synthetic and naturally occurring, has a pH dependant surface charge. Charge development occurs due to direct proton transfer to and from the surface hydroxyl groups. The point of zero charge (PZC) represents the pH at which the surface charge of the mineral is effectively zero and is also the pH at which a change occurs in the surface characteristics of the particle. At pH values below the PZC, the mineral surface is positively charged and at values above, the surface becomes negatively charged. As mentioned previously, the PZC also serves as a point of reference from which to characterize the stability of the particle suspension. The PZC was determined from zeta potential measurements and is presented in Figure 2, which shows the relationship between zeta potential and pH. The pH at which the zeta potential is zero approximates

the PZC for the system. Previous research has reported PZCs for synthetic magnetite at pH values ranging from 6-8 [19, 24, 29]. The PZC determined for the magnetite in this project was determined to be at pH = 6.5 +/ 0.25. This value suggests that pH mediated aggregation will occur to the greatest extent at pH values ranging from 6-7 and dispersion will increase the further a suspension is from this pH range.

Previous research has shown that the dechlorination of carbon tetrachloride by bulk magnetite is strongly influenced by the pH of the solution [19]. Danielsen and Hayes observed an increase in reaction rate with increasing pH over the range of 6-10. The pH values analyzed in this study were limited to the pH range of 6-8; the range available for HEPES buffered solutions. The observed dechlorination rates for our nanomagnetite solutions measured within this pH range, were again strongly pH dependent, but were significantly faster than the rates reported by Danielsen and Hayes. A comparison of the k_M and k_{SA} values from this study versus those from Danielsen and Hayes is shown in Figures 7a and 7b, respectively. The k_M values determined from the mass loading experiments (depicted in Figure 5) are presented along with the pH data, shown in Figure 7a. The similarity of the k_M values determined from the mass loading and the pH experiments (where only a single magnetite concentration was employed) corroborates the calculated reaction rates. Figures 7a and 7b relate distinct differences in CT dechlorination in the presence of magnetite between this study and that by Danielsen and Hayes. Since these differences are not resolved by either mass or surface area normalization, it can be inferred that there is another mechanism active in nanomagnetite solutions that causes increased reactivity towards carbon tetrachloride. One possible explanation for this behavior is that nanomagnetite particles are generally more stable in solution than are bulk particles. As a result, the reactive surfaces of nanoparticles may remain more accessible for reactions than the bulk particles.

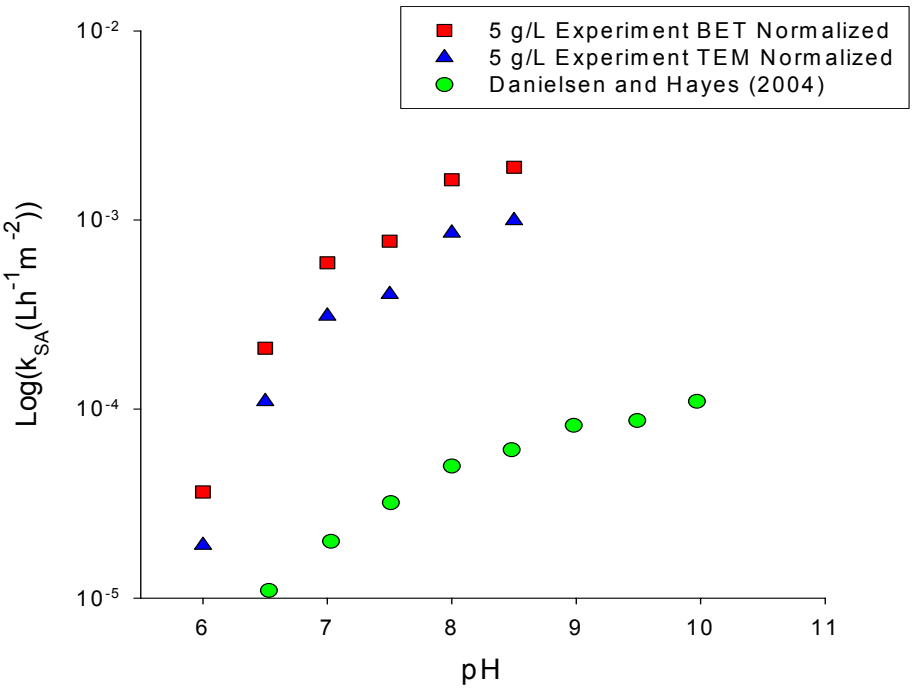

A)

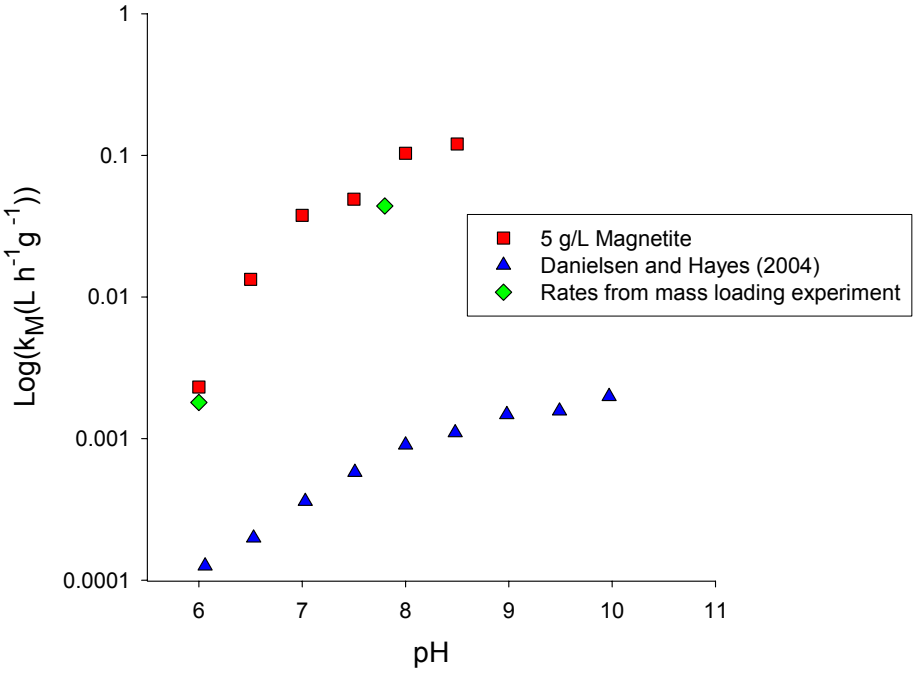

B)

Figure 7. Normalized, carbon tetrachloride reduction rate constants A) Mass normalized and B) Surface area normalized as a function of pH. $[CT]_0$ = 100 µM, 0.001 M NaCl and 50 mM HEPES.

Danielsen and Hayes attributed the reaction pH dependence shown in Figure 7, primarily to deprotonation-protonation reactions occurring at the mineral surface. Our results support this conclusion; however, we also suggest that pH mediated aggregation may influence the reaction rates. The reaction rates are the slowest at pH = 6 with only a slight increase at pH=6.5. However, the rates increase dramatically as the pH increases out of the pH 6-6.5 range

Ionic Strength Effects

The ionic strength of the aqueous solution has been shown to strongly influence particle aggregation [24, 29]. Colloidal interactions in solutions can be largely explained by the DLVO theory. Counter ions surround the charged particle surface in order to maintain electroneutrality within the solution[18]. The charged surface and the surrounding layer of counter ions form what is commonly called the electric double layer (EDL) [18]. The stability of a nanoparticle suspension is directly related to the magnitude or structure of the EDL. When the EDL is large, the suspension remains stable because particle-particle repulsion is also large. When the EDL is small, then the particle-particle repulsive forces are smaller as well and the particles are able to get closer to one another. When the particles are in close proximity to one another, van der Waals interactions promote particle aggregation. The ionic strength of the aqueous solution has a direct influence on the size and structure of the EDL. Increasing the ionic strength of a solution increases the background electrolyte concentration, which effectively decreases the size of the EDL. So in general, particle aggregation varies inversely with the ionic strength of the aqueous solution [30].

Sodium chloride and sodium perchlorate are indifferent electrolytes, meaning that they do not take part in reactions occurring at the mineral surface; however, Sun et al. concluded that the presence of multivalent cations that specifically adsorb to the particle surface could dramatically influence the aggregation behavior [29]. In this project we studied ionic strength effects on reaction rates by using three different electrolytes: sodium chloride (NaCl), calcium chloride ($CaCl_2$), and

sodium perchlorate ($NaClO_4$) at concentrations ranging from 0.001 M to 1 M at a pH of 7.8. At the lowest concentration (0.001 M), there were significant differences observed in CT reactivity rates due to the presence of the different electrolytes as shown in Figure 8a. Rates were slowest for reactions in which $CaCl_2$ set the ionic strength and increased in the order of $CaCl_2$< NaCl < $NaClO_4$. However, as the concentration of added electrolytes increased, the differences in k_{obs} values become smaller and at the highest ionic strength tested (1 M), there was no significant difference in the CT reaction rates. The differences in CT reactivity between NaCl and $NaClO_4$, the two monovalent salts, are most likely due to their respective sizes in solution[30]. The perchlorate anion has a larger molecular size than does chloride, which suggests, that in solution, perchlorate will promote larger particle separation than chloride. The increased particle separation better shields individual magnetite particles and results in a more dispersed suspension than solutions containing chloride.

The properties of the electrolyte in solution did not appear to influence the chloroform formation rates (see Figure 8b). For the three salts tested there was no significant difference in the CF formation rates at a given ionic strength. However, comparing the chloroform yields, (Table 2) illustrates that CF formation did follow the same trend as observed for the CT reduction rates. CF yield was greatest in solutions containing $NaClO_4$ and decreased in the order of $NaClO_4$ > NaCl >$CaCl_2$. Equation 8 presents the relationship used to calculate chloroform yield:

$$Y_{CF}(\%) = \frac{[CF]_{t=final}}{[CT]_{t=initial}} \times 100 \qquad \textbf{(Equation 8)}$$

The findings from the kinetic experiments conducted with pH and ionic strength variations show that CT reactivity in the presence of magnetite is strongly influenced by particle aggregation. For both conditions, CT reactivity was shown to increase with increasing dispersion potential. When pH effects were considered, the particles were predicted to agglomerate to the greatest extent around a ~ pH=6.5,which corresponded to the lowest range for measured kinetic rates. While the dispersion potential of the suspension was anticipated to increase with increasing ΔpH, as did the reaction rates.

For systems of variable ionic strength, particle suspensions were shown by previous research to be most stable at low ionic strength and agglomerated at high pH values. Again the reactivity of the system followed that agglomeration/dispersion trend. Based on these relationships it can be inferred that a dispersed magnetite suspension is more reactive towards CT than an agglomerated suspension. This difference is due to the increased surface availability of the particles in a dispersed system compared to an agglomerated system. These aggregation effects overlay the previously discussed protonation-deprotonation effects described by Danielsen and Hayes.

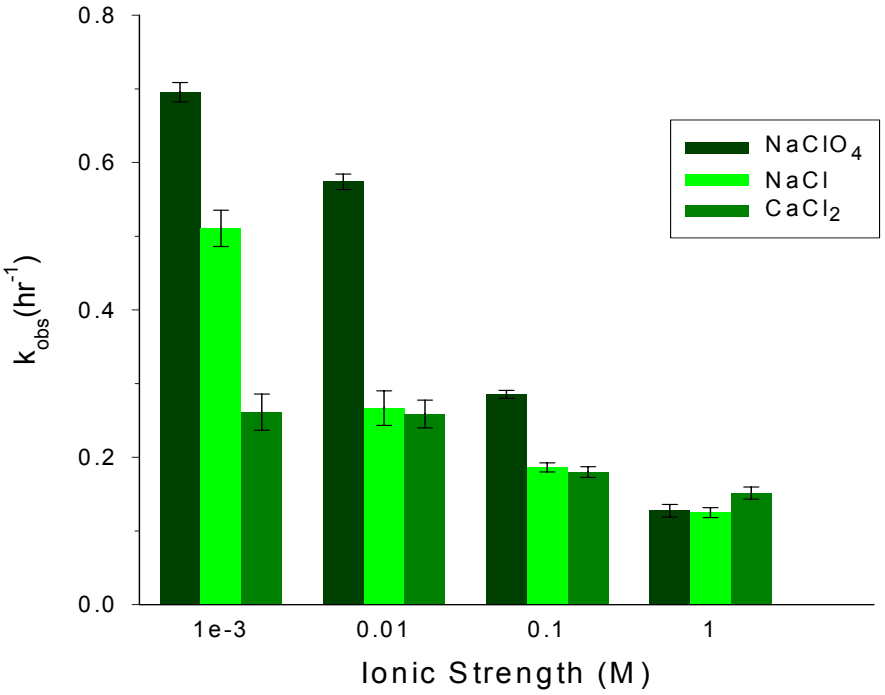

A)

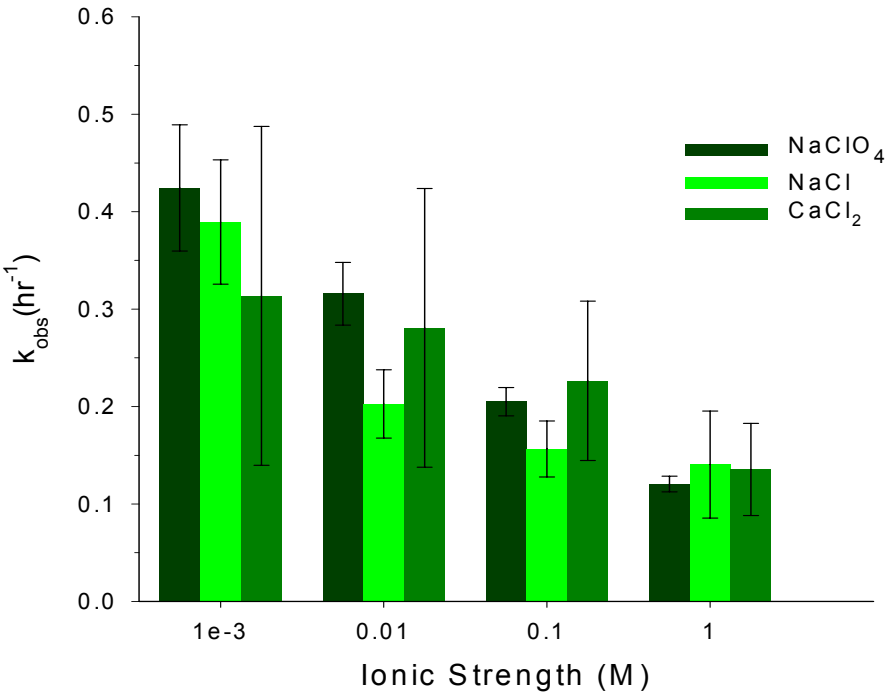

B)

Figure 8. Effect of ionic composition on the pseudo-first order rate constants A) carbon tetrachloride dechlorination and B) chloroform production rate. $[CT]_0$ = 100 µM, pH =7.8, 5 g/L nanomagnetite, 50 mM Hepes buffer.

Table 2. Chloroform yield percentages with corresponding electrolyte component and concentration.

Electrolyte / Ionic Strength (M)	Sodium Perchlorate	Sodium Chloride	Calcium Chloride
0.001	97.1	93.6	78.0
0.01	101.7	93.8	79.7
0.1	100.5	85.1	69.8
1.0	99.9	65.1	66.8

Temperature

Over the temperature range analyzed (3.6 to 36 °C), there was an increase in the observed rate constants for CT dechlorination and CF formation with an increase in temperature. The activation energy for the system was calculated by use of the Arrhenius Equation:

$$\ln k_{obs} = -\frac{E_a}{RT} + A \qquad \textbf{(Equation 9)}$$

Where k_{obs} is the observed pseudo-first-order rate constant, T is the temperature in Kelvin, R is the universal gas constant (8.314 J/mol K), E_a is the activation energy in J/mol, and A is a constant. The activation energy was calculated by multiplying the slope of the linear relationship (between the plot of natural log of the observed rate versus inverse temperature) by the universal gas constant (Figure 9). The activation energies for carbon tetrachloride loss and chloroform formation, were calculated to be 102.6 kJ/mol and 97.7 kJ/mol respectively, for the system of 5 g/L magnetite, at a pH =7.8 with an initial CT concentration of approximately 100 µM. These values were calculated from the reactions utilizing water bath mixing as opposed to the roller mixer regime due to the comparative number of temperatures analyzed by the different strategies (i.e., 3 versus 2 temperatures points). The Arrhenius relationships developed for both mixing regimes are shown in Figure 9. Based on the

comparison of the two data sets, it can be inferred that different mixing techniques provide different mixing intensities that affect the measured kinetic values

Previous research with zero-valent iron particles has reported activation energies for carbon tetrachloride dechlorination to be ~ 50 kJ/mol [9, 14]. Comparing the activation energies for these two iron species shows that more energy is required for magnetite to reductively dehalogenate carbon tetrachloride than for zero-valent iron. This may explain why in previous studies, zero-valent iron was able to reduce trichloroethylene and yet no reduction was shown to occur in the presence of magnetite [9].

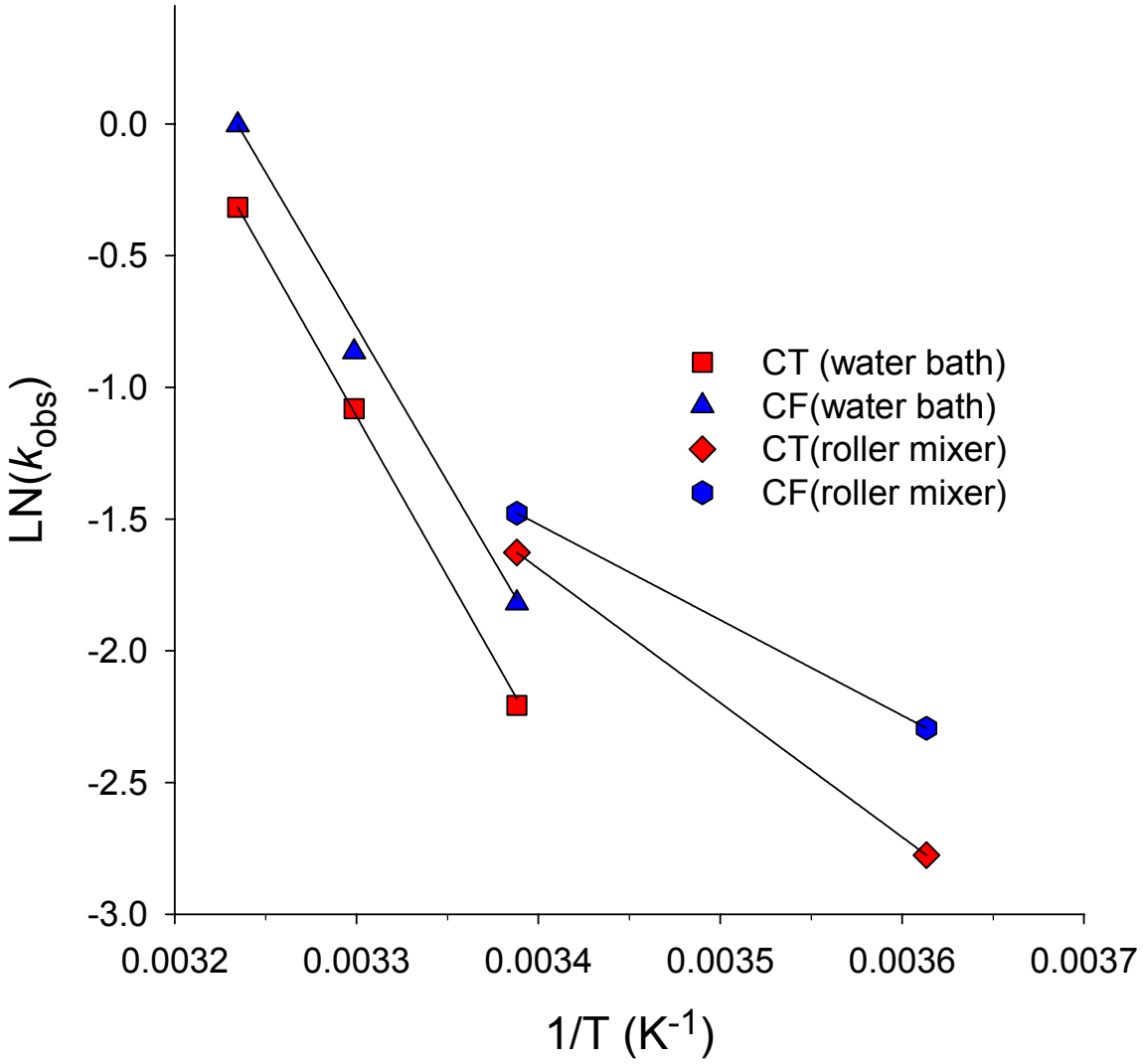

Figure 9. Arrhenius plot of the carbon tetrachloride and chloroform temperature rate dependence.

CONCLUSIONS

Magnetite nanoparticles readily degrade carbon tetrachloride in anaerobic environments. The rates of these reactions are a function of the magnetite concentration, pH, ionic strength, and the temperature of the system.

- Reaction rates were shown to vary linearly with increasing particle concentration. This relationship corroborated the first-order rate assumptions made in the kinetic model developed for this system.
- Solution pH influenced the dechlorination reactions by influencing the particle surface chemistry. Reaction rates increased with increasing pH due to surface protonation-deprotonation, which in turn directly influences the stability of the suspension.
- Both the background electrolyte concentration and composition appear to strongly influence the reaction kinetics. Over the range of ionic strength values analyzed, the reaction rates decreased with increasing ionic strength. The suspension stability was also dependent upon the ionic strength of the solution wherein the aggregation potential of the particle suspension increased with increasing ionic strength. Based on these observations it can be inferred that the reaction rates are influenced by the stability of the suspension where reactions occur significantly faster in the presence of dispersed particles as opposed to aggregated particles. The specific electrolyte present in solution also appears to influence reaction kinetics. Of the three salts analyzed, solutions containing the monovalent electrolytes sodium perchlorate and sodium chloride displayed significantly faster reaction rates than did solutions containing the divalent electrolyte calcium chloride.
- Reaction kinetics increased proportionally with temperature. Activation energies were determined for CT dechlorination and CF formation reactions through the Arrhenius relationship.

LITERATURE CITED

1. Westrick, J. J., Mello, J. W., and Thomas, R. F., *The groundwater supply survey.* J. American Water Works Assoc., 1984. **76**(5): p. 52-59.
2. McCarty, E. J. B. a. P. L., *Transformations of 1- and 2-carbon halogenated aliphatic organic compounds under methanogenic conditions.* Applied and Environmental Microbiology, 1983. **45**(4): p. 1286-1294.
3. McCormick, M. L. and Adriaens, P., *Carbon tetrachloride transformation on the surface of nanoscale biogenic magnetite particles.* Environ. Sci. Technol., 2004. **38**(4): p. 1045-1053.
4. McCormick, M. L., Bouwer, E. J., and Adriaens, P., *Carbon tetrachloride transformation in a model iron-reducing culture: Relative kinetics of biotic and abiotic reactions.* Environ. Sci. Technol., 2002. **36**(3): p. 403-410.
5. Amonette, J. E., Workman, D. J., Kennedy, D. W., Fruchter, J. S., and Gorby, Y. A., *Dechlorination of carbon tetrachloride by Fe(II) associated with goethite.* Environ. Sci. Technol., 2000. **34**(21): p. 4606-4613.
6. Elsner, M., Schwarzenbach, R. P., Kellerhals, T., Luzi, S., Zwank, L., Angst, W., and Haderlein, S. B., *Mechanisms and products of surface-mediated reductive dehalogenation of carbon tetrachloride by Fe(II) on goethite.* Environ. Sci. Technol., 2004. **38**(7): p. 2058-2066.
7. Erbs, M., Bruun Hansen, H. C., and Olsen, C. E., *Reductive dechlorination of carbon tetrachloride using Fe(II) Fe(III) hydroxide sulfate (green rust).* Environ. Sci. Technol., 1999. **33**(2): p. 307-311.
8. Johnson, T. L., Fish, W., Gorby, Y. A., and Tratnyek, P. G., *Degradation of carbon tetrachloride by iron metal: Complexation effects on the oxide surface.* J. Cont. Hydrology, 1998. **29**(4): p. 379-398.
9. Li, T. and Farrell, J., *Electrochemical investigation of the rate-limiting mechanisms for trichloroethylene and carbon tetrachloride reduction at iron surfaces.* Environ. Sci. Technol., 2001. **35**(17): p. 3560-3565.
10. O'Loughlin, E. J., Kemner, K. M., and Burris, D. R., *Effects of Ag(I),Au(III), and Cu(II) on the reductive dechlorination of carbon tetrachloride by green rust.* Environ. Sci. Technol., 2003. **37**(13): p. 2905-2912.
11. Pecher, K., Haderlein, S. B., and Schwarzenbach, R. P., *Reduction of polyhalogenated methanes by surface-bound fe(ii) in aqueous suspensions of iron oxides.* Environ. Sci. Technol., 2002. **36**(8): p. 1734-1741.
12. Reinhard, M. R. K.-K. a. M., *Transformation of carbon tetrachloride in the presence of sulfide, biotite, and vermiculite.* Environ. Sci. Technol., 1992. **26**(11): p. 2198-2206.
13. Reinhard, M. R. K.-K. a. M., *Transformation of carbon tetrachloride by pyrite in aqueous solution.* Environ. Sci. Technol., 1994. **28**(4): p. 692-700.
14. Scherer, M. M., Westall, J. C., Ziomek-Moroz, M., and Tratnyek, P. G., *Kinetics of carbon tetrachloride reduction at an oxide-free iron electrode.* Environ. Sci. Technol., 1997. **31**(8): p. 2385-2391.
15. Joerg Klausen, S. P. T., Stefan B. Haderlein, Rene P. Schwarzenbach, *Reduction of substituted nitrobenzenes by Fe(II) in aqueous mineral suspensions.* Environ. Sci. Technol., 1995. **29**(9): p. 2396-2404.
16. Kohn, T., Livi, K. J. T., Roberts, A. L., and Vikesland, P. J., *Longevity of granular iron in groundwater treatment processes: Corrosion product development.* Environ. Sci. Technol., 2005. **39**(8): p. 2867-2879.

17. Lien, H.-L. and Zhang, W., *Nanoscale iron particles for complete reduction of chlorinated ethenes.* Colloids and Surfaces A: Physicochemical and Engineering Aspects, 2001. **191**(1-2): p. 97-105.
18. R.M Cornell, U. S., *The iron oxides structures, properties, reactions, occurences and uses*. Second ed. 2003, Weinheim, Germany: VCH. 402-404, 232-235.
19. Danielsen, K. M. and Hayes, K. F., *pH dependence of carbon tetrachloride reductive dechlorination by magnetite.* Environ. Sci. Technol., 2004. **38**(18): p. 4745-4752.
20. Zaitsev, V. S., Filimonov, D. S., Presnyakov, I. A., Gambino, R. J., and Chu, B., *Physical and chemical properties of magnetite and magnetite-polymer nanoparticles and their colloidal dispersions.* J. Colloid and Interface Sci., 1999. **212**(1): p. 49-57.
21. Zhang, W., *Nanoscale iron particles for environmental remediation: An overview.* J. Nanoparticle Research, 2003. **5**(3 - 4): p. 323-332.
22. Vayssieres, L. C., C;Tronc, E; Jolivet,J.P, *Size tailoring of magnetite particles formed by aqueous precipitation: An example of thermodynamic stability of nanometric iron oxide particles.* J. Colloid and Interface Sci., 1998. **205**: p. 205-212.
23. Penn, R. L., Oskam, G., Strathmann, T. J., Searson, P. C., Stone, A. T., and Veblen, D. R., *Epitaxial assembly in aged colloids.* J. Phys. Chem. B, 2001. **105**(11): p. 2177-2182.
24. Tombacz, E., Csanaky, C., and Illes, E., *Polydisperse fractal aggregate formation in clay mineral and iron oxide suspensions, ph and ionic strength dependence.* Colloid & Polymer Sci., 2001. **279**(5): p. 484-492.
25. Danielsen, K. M., Gland, J. L., and Hayes, K. F., *Influence of amine buffers on carbon tetrachloride reductive dechlorination by the iron oxide magnetite.* Environ. Sci. Technol., 2005. **39**(3): p. 756-763.
26. McCarty, C. S. C. a. P. L., *Electrolytic model system for reductive dehalogenation in aqueous environments.* Environ. Sci. Technol., 1991. **25**(5): p. 973-978.
27. Buzmakov, V. M. and Pshenichnikov, A. F., *On the structure of microaggregates in magnetite colloids.* J. Colloid and Interface Sci., 1996. **182**(1): p. 63-70.
28. Nurmi, J. T., Tratnyek, P. G., Sarathy, V., Baer, D. R., Amonette, J. E., Pecher, K., Wang, C., Linehan, J. C., Matson, D. W., Penn, R. L., and Driessen, M. D., *Characterization and properties of metallic iron nanoparticles: Spectroscopy, electrochemistry, and kinetics.* Environ. Sci. Technol., 2005. **39**(5): p. 1221-1230.
29. Sun, Z.-X., Su, F.-W., Forsling, W., and Samskog, P.-O., *Surface characteristics of magnetite in aqueous suspension.* J. Colloid and Interface Sci., 1998. **197**(1): p. 151-159.
30. Colic, M., Fisher, M. L., and Franks, G. V., *Influence of ion size on short-range repulsive forces between silica surfaces.* Langmuir, 1998. **14**(21): p. 6107-6112.

APPENDIX A

Yield Calculations

Batch Yield

In the presence of oxygen, magnetite (Fe_3O_4) is converted to maghemite (γ-Fe_2O_3), The following calculations assume 100% conversion of $Fe_3O_4 \rightarrow \gamma$-$Fe_2O_3$ during the oven drying process.

Stoichiometric Relationship : $4Fe_3O_4 + O_2 \rightarrow 6Fe_2O_3$ (1)

$$\gamma\text{-}Fe_2O_3 \text{ Mass (g)} = \text{Oven Dry Wt of Particles} \quad (2)$$

$$Fe_3O_4\,(g) = Fe_2O_3\,(g) \times \frac{1}{MW\,(Fe_2O_3)} \times \text{StoichiometricRatio}\,\frac{Fe_3O_4}{Fe_2O_3} \times MW(Fe_3O_4) \quad (3)$$

Values: MW Fe_2O_3 = 159.7 g/mol
MW Fe_3O_4 = 231.55 g/mol
Stoich. Ratio = 4:6

→ Magnetite (Particle) Concentration is determined by dividing the calculated magnetite mass (from equation 3) by the aliquot volume.

Maximum Yield

→ This calculation assumes that Fe^{2+} is the limiting reactant

$$\text{Maximum yield of } Fe_3O_4\,(g) = [(\text{Vol.of } Fe^{2+}\,(L)) \times (\text{Conc. of } Fe^{2+} \text{ soln (M)}) \times (\text{Molar ratio of } \frac{Fe^{2+}}{Fe_3O_4}) \times (\text{MW of } Fe_3O_4 \text{ (g/mol)})] \quad (4)$$

$$\text{Maximum Slurry Concentration (g/L)} = \frac{\text{Max yield - } Fe_3O_4\,(g)}{\text{Total Vol. of Slurry(L)}} \quad (5)$$

Example Calc: Calculate (g) of Fe_3O_4 in single particle batch :

$$Fe_3O_4\,(g) = 0.3\text{ L } Fe^{2+} \times \frac{0.1\text{ mol}}{\text{L}} \times \frac{1\text{ mol } Fe^{2+}}{1\text{ mol } Fe_3O_4} \times 231.55\,\frac{\text{g}}{\text{mol}}\,Fe_3O_4 = 6.95\text{ g}$$

Appendix B

Degradation And Formation Relationships

Synthesis Reproducibility

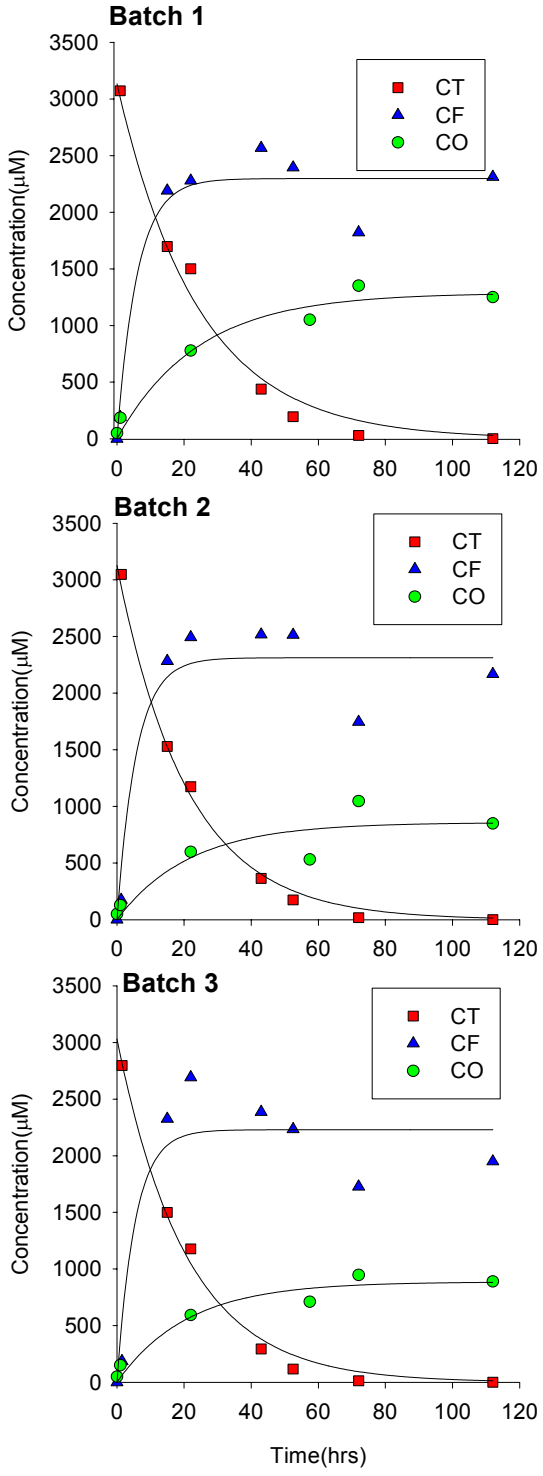

Figure 10. Synthesis Reproducibility: $[CT]_0$ = 3 mM, pH 7, 0.001 M NaCl, 50 mM HEPES
k_{obs} [(CT), (CF)] = (I) [0.0412 hr^{-1}, 0.165 hr^{-1}], (II) [0.048 hr^{-1},0.174 hr^{-1}], (III) [0.048 hr^{-1}, 0.0461 hr^{-1}]

Temperature Dependence:

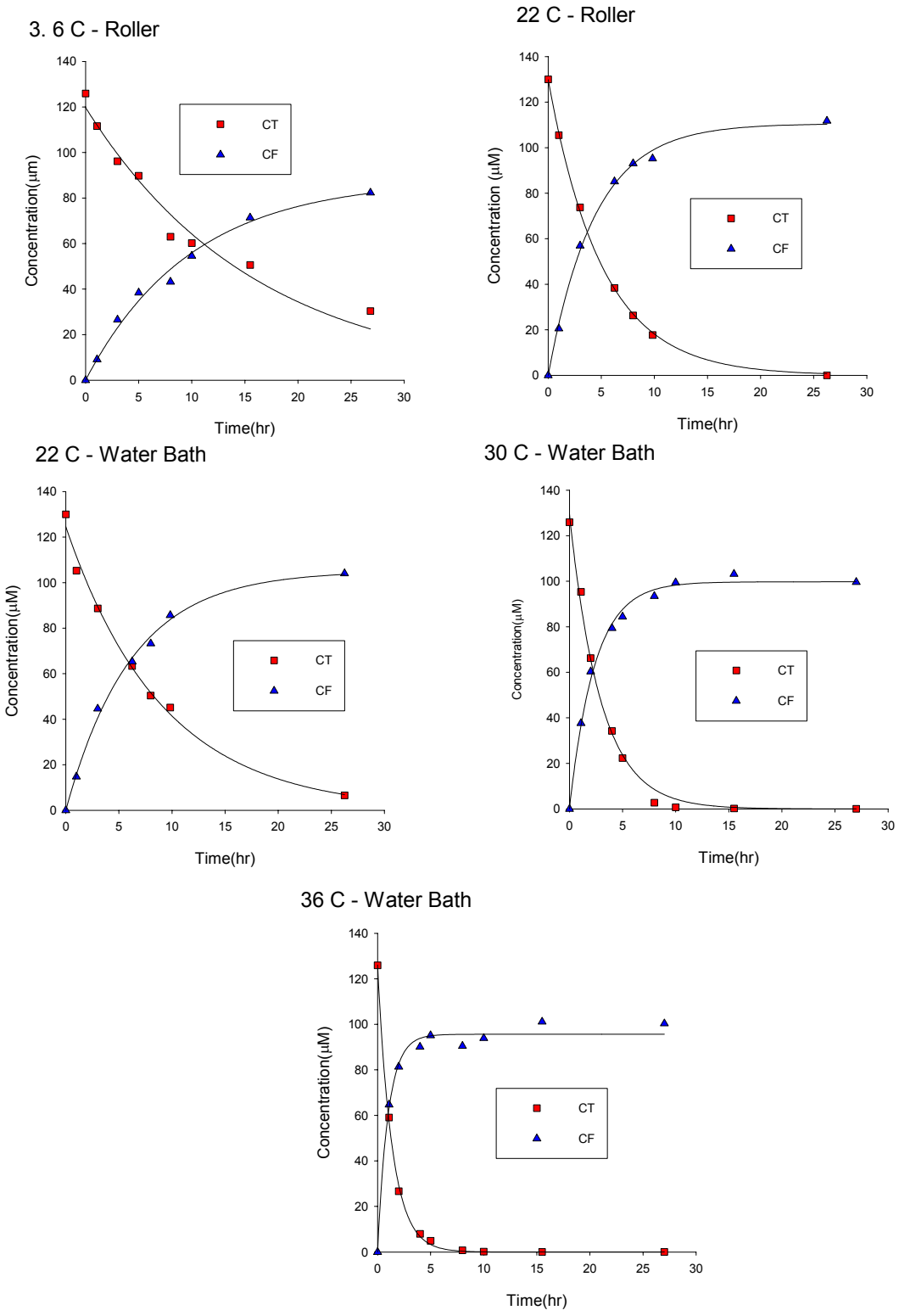

Figure 11. Temperature Dependence: $[CT]_0$ = 100 µM, 5 g/L Magnetite, 0.001 M NaCl, pH 7.8, 50 mM HEPES

(k_{obs} [(CT), (CF)] = (3.6 °C, Roller) [0.062 hr^{-1}, 0.101 hr^{-1}], (22 °C, Roller) [0.197 hr^{-1}, 0.228 hr^{-1}], (22 °C, Water bath) [0.110 hr^{-1}, 0.162 hr^{-1}], (30 °C, Water bath) [0.339 hr^{-1}, 0.421 hr^{-1}], (30 °C, Water bath) [0.729 hr^{-1}, 0.996 hr^{-1}])

Ionic Strength Dependence

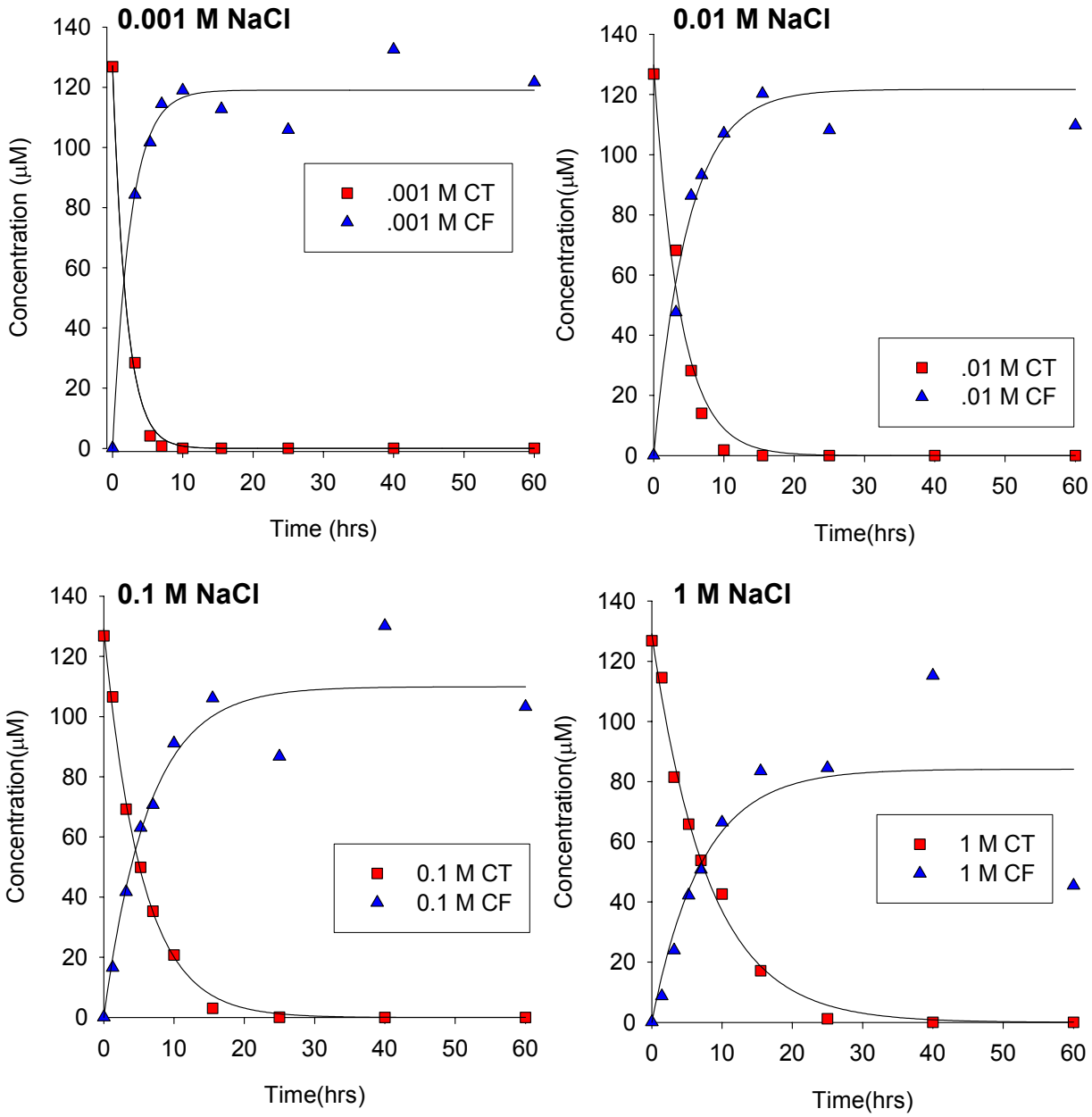

Figure 12. Ionic Strength Dependence: Sodium Chloride: $[CT]_0 = 100$ µM, 5 g/L Magnetite, pH 7.8, 50 mM HEPES

(k_{obs} [(CT), (CF)] = (0.001 M) [0.511 hr^{-1}, 0.389 hr^{-1}], (0.01 M) [0.267 hr^{-1}, 0.203 hr^{-1}], (0.1 M) [0.186 hr^{-1}, 0.156 hr^{-1}], (1.0 M) [0.125 hr^{-1}, 0.140 hr^{-1}])

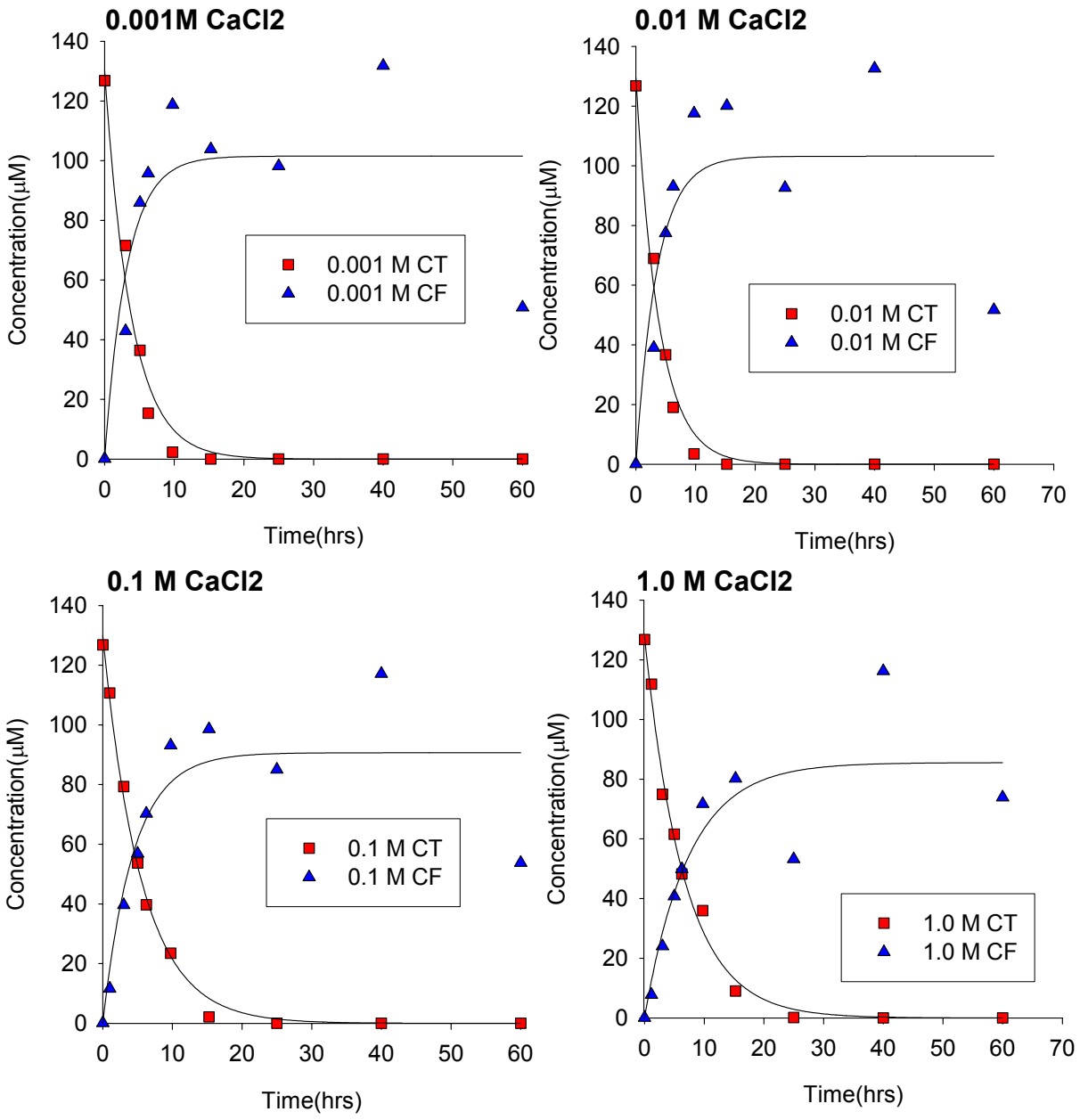

Figure 13. Ionic Strength Dependence: Calcium Chloride: $[CT]_0 = 100$ µM, 5 g/L Magnetite, pH 7.8, 50 mM HEPES.

(k_{obs} [(CT), (CF)] = (0.001 M) [0.261 hr^{-1}, 0.313 hr^{-1}], (0.01 M) [0.256 hr^{-1} , 0.281 hr^{-1}], (0.1 M) [0.180 hr^{-1}, 0.226 hr^{-1}], (1.0 M) [0..151 hr^{-1}, 0.135 hr^{-1}])

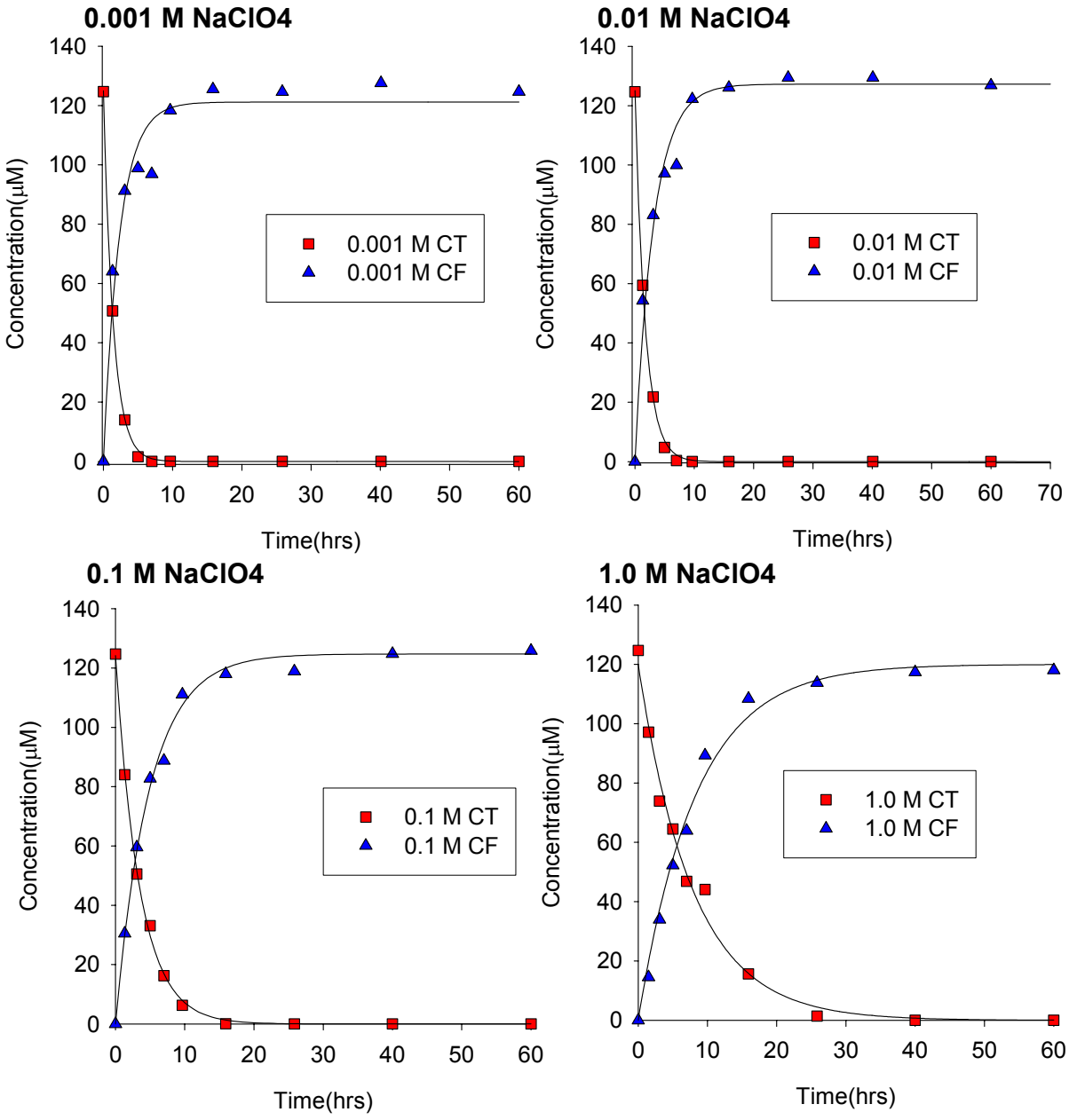

Figure 14. Ionic Strength Dependence: Sodium Perchlorate: $[CT]_0$ = 100 µM, 5 g/L Magnetite, pH 7.8, 50 mM HEPES

(k_{obs} [(CT), (CF)] = (0.001 M) [0.696 hr^{-1}, 0.424 hr^{-1}], (0.01 M) [0.574 hr^{-1} , 0.316 hr^{-1}], (0.1 M) [0.285 hr^{-1}, 0.205 hr^{-1}], (1.0 M) [0.127 hr^{-1}, 0.121 hr^{-1}])

Mass Loading Dependence

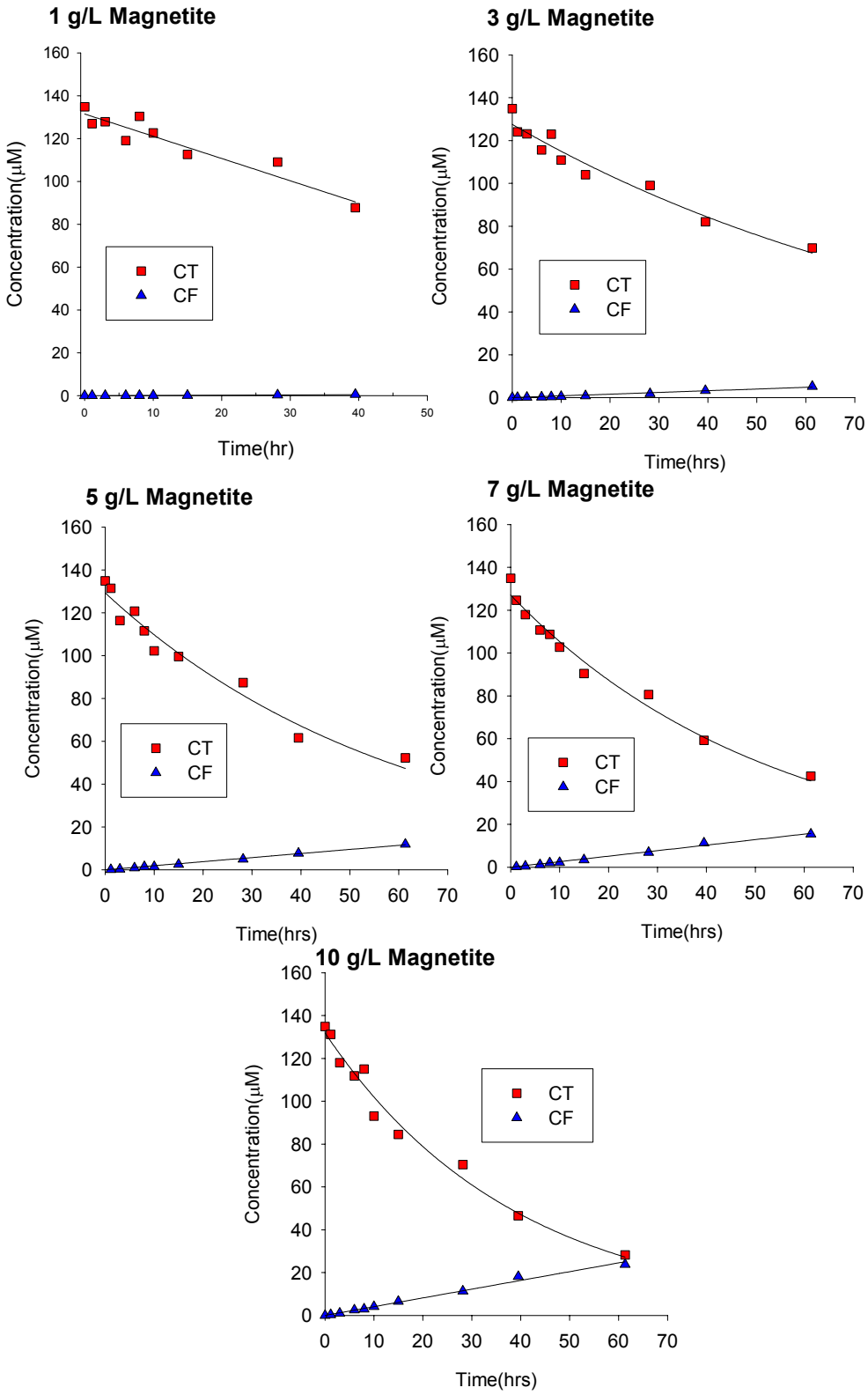

Figure 15. Mass Loading: pH 6, $[CT]_0 = 100$ μM, 0.001 M NaCl, 50 mM HEPES
(k_{obs} [(CT), (CF)] = (1 g/L) [0.009 hr^{-1}, 3.46 × 10^{-6} hr^{-1}], (3 g/L) [0.010 hr^{-1} , 1.84 × 10^{-6} hr^{-1}], (5 g/L) [0.016 hr^{-1}, 1.7 × 10^{-6} hr^{-1}], (7 g/L) [0.019 hr^{-1}, 1, 2 × 10^{-6} hr^{-1}], (10 g/L) [0.026 hr^{-1}, 3.17× 10^{-6} hr^{-1}])

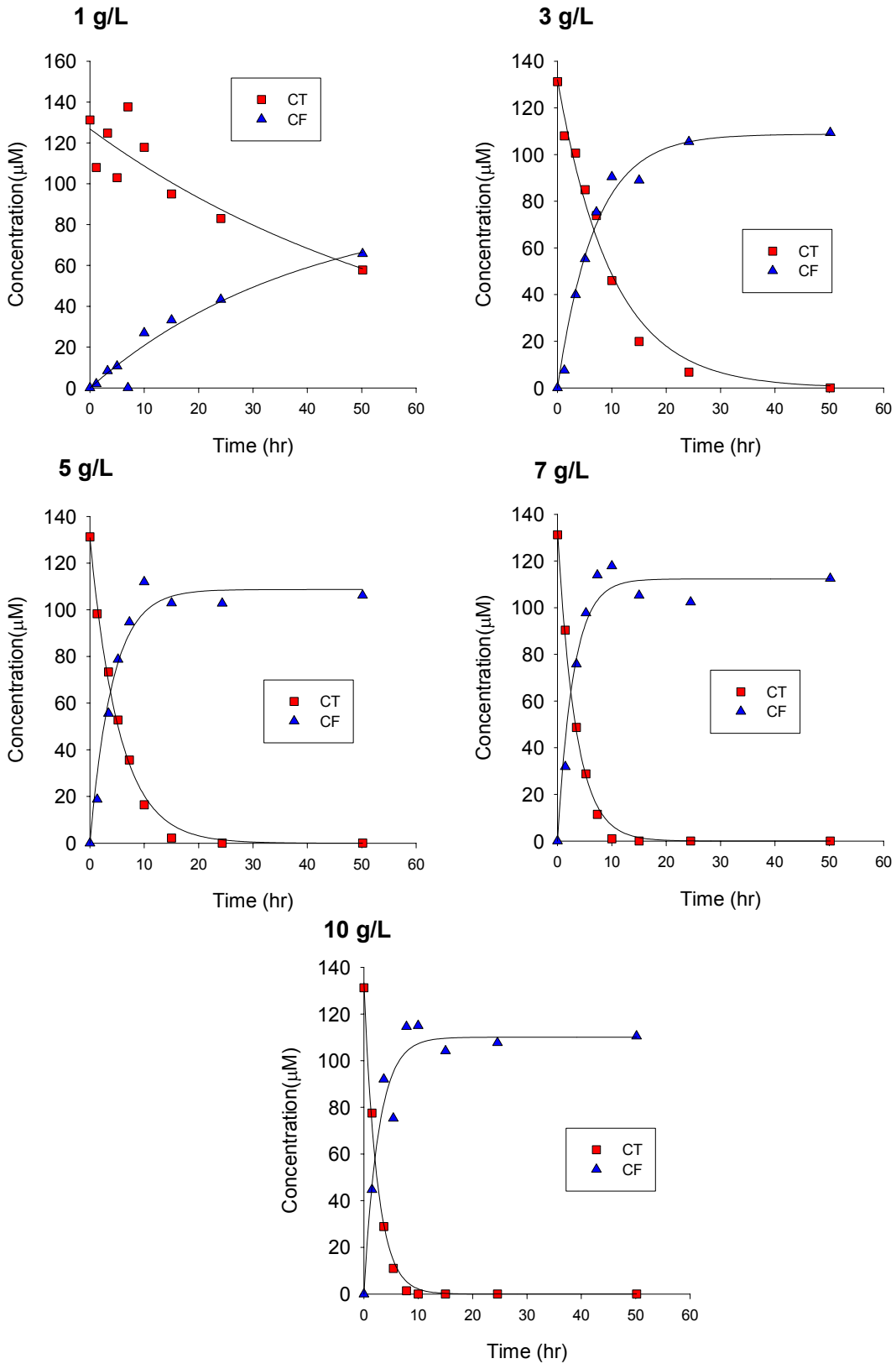

Figure 16. Mass Loading Dependence: pH = 7.8, $[CT]_0$ = 100 μM, 0.001 M NaCl, 50 mM HEPES

(k_{obs} [(CT), (CF)] = (1 g/L) [0.016 hr^{-1}, 0.026 hr^{-1}], (3 g/L) [0.010 hr^{-1}, 0.145 hr^{-1}], (5 g/L) [0.186 hr^{-1}, 0.240 hr^{-1}], (7 g/L) [0.298 hr^{-1}, 0.341 hr^{-1}], (10 g/L) [0.409 hr^{-1}, 0.368 hr^{-1}])

pH Dependency

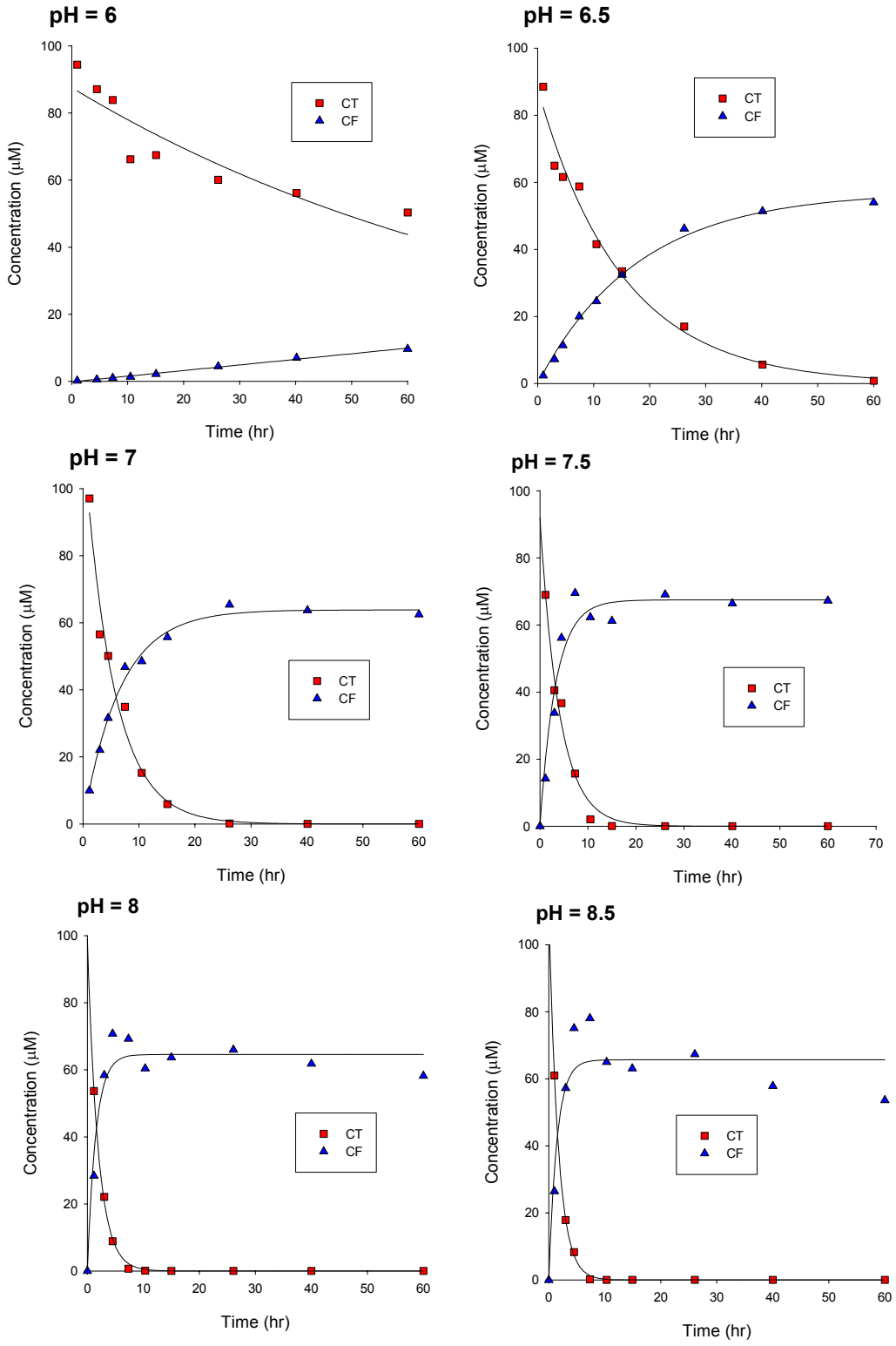

Figure 17. pH Dependence: $[CT]_0$ = 100 µM, 0.001 M NaCl, 5 g/L Magnetite, 50 mM HEPES. (k_{obs} [(CT), (CF)] = (pH = 6) [0.012 hr^{-1}, 0.061 hr^{-1}], (pH = 6.5) [0.067 hr^{-1} ,0.057 hr^{-1}], (pH = 7) [0.189 hr^{-1}, 0.151 hr^{-1}], (pH = 7.5) [0.246 hr^{-1}, 0.302 hr^{-1}], (pH = 8) [0.518 hr^{-1}, 0.663 hr^{-1}], (pH = 8.5) [0.603 hr^{-1}, 0.687 hr^{-1}])

VITA

April Marie Heathcock was born in Gadsden, Alabama on April 12, 1980 to Alan and Elizabeth Heathcock. She attended Auburn University from the fall 1999 to fall 2003 where she earned a B.S. in Civil Engineering. She obtained EIT certification in the fall of 2002. After graduation, she pursued interests in graduate studies while working at Botega Café in Birmingham, Alabama. In August 2005, she began her graduate studies at Virginia Polytechnic Institute and State University in Blacksburg, Virginia. Her M.S. ENE degree was completed in August 2006 and she is presently working for Joyce Engineering in Richmond, Virginia.